

PHOTOCATALYTIC ACTIVITY OF APATITE-DEPOSITED TITANIUM DIOXIDE
POWDER

A THESIS SUBMITTED TO
THE GRADUATE SCHOOL OF NATURAL AND APPLIED SCIENCES
OF
MIDDLE EAST TECHNICAL UNIVERSITY

BY

KAAN SOYSAL

IN PARTIAL FULFILLMENT OF THE REQUIREMENTS
FOR
THE DEGREE OF MASTER OF SCIENCE
IN
METALLURGICAL AND MATERIALS ENGINEERING

APRIL 2010

Approval of the thesis:

**PHOTOCATALYTIC ACTIVITY OF APATITE-DEPOSITED TITANIUM
DIOXIDE POWDER**

submitted by **KAAN SOYSAL** in partial fulfillment of the requirements for the degree of **Master of Science in Metallurgical and Materials Engineering Department, Middle East Technical University** by,

Prof. Dr. Canan Özgen, _____
Dean, Graduate School of **Natural and Applied Sciences**

Prof. Dr. Tayfur Öztürk, _____
Head of Department, **Metallurgical and Materials Engineering**

Prof. Dr. Abdullah Öztürk, _____
Supervisor, **Metallurgical and Materials Engineering Dept., METU**

Examining Committee Members:

Prof. Dr. Muharrem Timuçin, _____
Metallurgical and Materials Engineering Dept., METU

Prof. Dr. Abdullah Öztürk, _____
Metallurgical and Materials Engineering Dept., METU

Assoc. Prof. Dr. Caner Durucan, _____
Metallurgical and Materials Engineering Dept., METU

Asst. Prof. Dr. H. Emrah Ünal, _____
Metallurgical and Materials Engineering Dept., METU

Asst. Prof. Dr. Jongee Park, _____
Materials Engineering Dept., Atılım University

Date: 26.04.2010

I hereby declare that all information in this document has been obtained and presented in accordance with academic rules and ethical conduct. I also declare that, as required by these rules and conduct, I have fully cited and referenced all material and results that are not original to this work.

Name, Surname : Kaan SOYSAL

Signature :

ABSTRACT

PHOTOCATALYTIC ACTIVITY OF APATITE-DEPOSITED TITANIUM DIOXIDE POWDER

Soysal, Kaan

M.S., Department of Metallurgical and Materials Engineering

Supervisor: Prof. Dr. Abdullah Öztürk

April 2010, 66 pages

Apatite was formed on the surface of titanium dioxide (TiO_2) powders by a biomimetic process. The deposition was accomplished by immersing TiO_2 powders in simulated body fluid (SBF) for 1, 3, 6, 12, and 24 h. SBF used throughout this study had calcium and phosphate ion concentrations 10 times greater than those of human blood plasma. Photocatalytic activity of the apatite-deposited TiO_2 powders was investigated in terms of the decomposition of methylene blue solution under ultraviolet (UV) irradiation. It has been shown that apatite deposition enhanced the photocatalytic activity of TiO_2 . The best photocatalytic performance was acquired on the powders that are immersed in SBF for 3 h. The time required for the complete degradation of methylene blue decreased from 3.5 h to 2 h upon immersion of powders in SBF for 3 h. Photochemical durability of poly(methyl methacrylate) increased when it was mixed with apatite-deposited TiO_2 powders.

Keywords: photocatalysis; titanium dioxide; hydroxyapatite; simulated body fluid; methylene blue solution; poly(methyl methacrylate)

ÖZ

APATİT-DEPOLANMIŞ TİTANYUM DİOKSİT TOZUNUN FOTOKATALİTİK AKTİVİTESİ

Soysal, Kaan

Yüksek Lisans, Metalurji ve Malzeme Mühendisliği Bölümü

Tez Yöneticisi: Prof. Dr. Abdullah Öztürk

Nisan 2010, 66 sayfa

Bir biyobenzetim işlemiyle titanyum dioksit (TiO_2) tozları üzerine apatit oluşturulmuştur. Depolama işlemi TiO_2 tozlarının yapay vücut sıvısında 1, 3, 6, 12, ve 24 saat tutarak gerçekleştirilmiştir. Bu çalışmada kullanılan yapay vücut sıvısı, insan kan plazmasından 10 kat daha fazla kalsiyum ve fosfat iyonu içermiştir. Apatit depolanmış TiO_2 tozlarının fotokatalitik etkinliği, metilen mavisi solüsyonun ultraviyole ışını altında bozunumu ile incelenmiştir. Apatit depolamanın TiO_2 tozlarının fotokatalitik etkinliğini arttırdığı saptanmıştır. En iyi fotokatalitik performans yapay vücut sıvısında 3 saat tutulan TiO_2 tozlarından elde edilmiştir. Metilen mavisinin tamamen yok olma süresi, yapay vücut sıvısında 3 saat tutulan TiO_2 tozları için, 3,5 saatten 2 saate düşmüştür. Polimetil metakrilatın fotokimyasal dayanıklılığı apatit depolanmış TiO_2 tozlarıyla karıştırıldığı zaman artmıştır.

Anahtar Kelimeler: fotokataliz; titanyum dioksit; hidroksiapatit; yapay vücut sıvısı; metilen mavisi solüsyonu; polimetilmetakrilat

To my family

ACKNOWLEDGEMENT

I would like to express my deepest gratitude to my supervisor Prof. Dr. Abdullah Öztürk, for his endless support, advice, encouragement, and patience. Without him, this thesis would not be here.

I would also like to thank to Asst. Prof. Dr. Jongee Park for his guidance and friendship throughout all the experiments and before.

I also wish to give my special thanks to my dear family and friends for their love, support, trust, and enthusiasm, who always make me feel like I'm privileged.

TABLE OF CONTENTS

ABSTRACT.....	iv
ÖZ.....	v
ACKNOWLEDGEMENT	vii
TABLE OF CONTENTS.....	viii
LIST OF TABLES.....	x
LIST OF FIGURES	xi
CHAPTER I: INTRODUCTION	1
CHAPTER II: LITERATURE REVIEW.....	4
2.1. PHOTOCATALYSIS.....	4
2.2. PHOTOCATALYTIC MATERIALS.....	8
2.2.1. Photocatalytic Titanium Dioxide (TiO ₂)	9
2.3. ENHANCEMENT of PHOTOCATALYTIC ACTIVITY of TiO ₂	10
2.4. APATITE DEPOSITION and SIMULATED BODY FLUID.....	11
2.5. METHYLENE BLUE (MB)	15
2.6. POLY (METHYLMETHACRYLATE) (PMMA).....	17
CHAPTER III: EXPERIMENTAL PROCEDURE.....	19
3.1. PROPERTIES of TITANIUM DIOXIDE (TiO ₂)	19
3.2. PREPARATION of SIMULATED BODY FLUID (SBF).....	20
3.3. APATITE DEPOSITION on TiO ₂ POWDERS.....	21
3.4. PREPARATION of the COMPACTS of PMMA and TiO ₂ POWDERS.....	23
3.5. CHARACTERIZATION.....	24
3.5.1. X-Ray Diffraction (XRD) and Fourie Transform Infrared Spectroscopy, FTIR, Analyses.....	24
3.5.2. Scanning Electron Microscope (SEM) and Energy Dispersive Spectroscopy (EDS) Analyses.....	24
3.6. PHOTOCATALYTIC ACTIVITY MEASUREMENTS.....	25
3.6.1. Photocatalytic Activity of the Compacts of PMMA and TiO ₂ Powders	25

3.6.2. Photocatalytic Activity of TiO ₂ Powders in Methylene Blue (MB) Solution	26
CHAPTER IV: RESULTS AND DISCUSSION	29
4.1. GENERAL	29
4.2. CHARACTERIZATION	29
4.2.1. X-Ray Diffraction (XRD) and Fourier Transform Infrared Spectroscopy (FTIR)	29
4.2.2. Scanning Electron Microscope (SEM) and Energy Dispersive Spectroscopy (EDS)	32
4.3. THE PHOTOCATALYTIC ACTIVITY	39
4.3.1. Photocatalytic Activity of the Compacts of PMMA and TiO ₂ Powders	39
4.3.2. Photocatalytic Activity of TiO ₂ Powders in Methylene Blue (MB) Solution	41
CHAPTER V: CONCLUSIONS	55
REFERENCES	56

LIST OF TABLES

TABLE 2. 1 Selected photocatalytic materials, their band gaps and wavelengths [35].....	8
TABLE 2. 2 Ion concentration in SBF and human blood plasma [54].....	13
TABLE 3. 1 Chemical and physical properties of TiO ₂ [69]	19
TABLE 3. 2 Ion Concentrations in human blood plasma, SBF and 10-SBF [70]	20
TABLE 3. 3 Weight percentages of reagents used for preparing 10-SBF	21
TABLE 4. 1 Weight percentage of hydroxyapatite on TiO ₂ powders	34
TABLE 4. 2 Weight concentrations of CaO and P ₂ O ₅ in TiO ₂ powders after immersion in SBF.....	34
TABLE 4. 3 Values for the reaction rate constant and correlation coefficient for the photocatalytic decomposition of MB.....	45
TABLE 4. 4 The reaction rate constant and correlation coefficient for unreacted TiO ₂ for different MB concentrations in the solution.....	47
TABLE 4. 5 The reaction rate constant for 3HAP-TiO ₂ of different MB concentrations in solution	49
TABLE 4. 6 The reaction rate constant and correlation coefficient for different amounts of unreacted TiO ₂ in the solution	51
TABLE 4. 7 The reaction rate constant and correlation coefficient for different amounts of 3HAP-TiO ₂ in the solution.....	54

LIST OF FIGURES

FIGURE 1. 1 Typical applications of photocatalytic TiO ₂ [9].....	2
FIGURE 2. 1 Schematic illustration of photocatalytic events [24].....	5
FIGURE 2. 2 Schematic illustration of the processes occurring during photocatalytic oxidation of CH ₃ CHO on an illuminated TiO ₂ particle [9]	7
FIGURE 2. 3 Schematic diagram showing the mechanism of apatite formation on TiO ₂ coating in SBF [59].....	14
FIGURE 2. 4 The structure of Methylene Blue [60]	15
FIGURE 2. 5 Structures of (a) PMMA, (b) PMA, and (c) methamphetamine [64]	17
FIGURE 3. 1 Flowchart showing the experimental procedure for apatite deposition on TiO ₂ powders	22
FIGURE 3. 2 Flowchart showing the experimental procedure for the preparation of the compacts composed of PMMA and TiO ₂ powders	23
FIGURE 3. 3 Flowchart showing the experimental procedure for the measurement of the photocatalytic activity of the compacts composed of PMMA and TiO ₂ powders	26
FIGURE 3. 4 Flowchart showing the experimental procedure for the measurement of the photocatalytic activity of the TiO ₂ powders in the MB solution	27
FIGURE 4. 1 XRD patterns of TiO ₂ powders before and after immersion in the 10-SBF	30
FIGURE 4. 2 FTIR spectra of a) unreacted TiO ₂ b) 1HAP-TiO ₂ , c) 3HAP-TiO ₂ and d) 6HAP-TiO ₂ powders.....	32
FIGURE 4. 3 SEM micrographs of a) unreacted TiO ₂ , b) 1HAP-TiO ₂ ,.....	33
FIGURE 4. 4 EDS analysis results for a) 1HAP-TiO ₂ , b) 3HAP-TiO ₂ ,	36
FIGURE 4. 5 Schematic diagram showing the possible mechanism of apatite formation on TiO ₂ powder in 10-SBF	38

FIGURE 4. 6 Percent weight change in the compacts of PMMA and TiO ₂ powders with UV exposure time.....	40
FIGURE 4. 7 Weight change in the compacts of PMMA and TiO ₂ powders with UV exposure time	41
FIGURE 4. 8 Variation in light absorption with UV exposure time for unreacted TiO ₂ and apatite deposited TiO ₂ powders	42
FIGURE 4. 9 Variation of percent MB concentration with UV exposure time for unreacted TiO ₂ and apatite deposited TiO ₂ powders	42
FIGURE 4. 10 Variation of $\ln([MB]_0/[MB])$ with UV exposure time for the unreacted and apatite deposited TiO ₂ powders	44
FIGURE 4. 11 Variation in light absorption with UV exposure time for different MB concentrations in the solution	46
FIGURE 4. 12 Variation of percent MB concentration with UV exposure time for different MB concentrations in the solution	46
FIGURE 4. 13 Variation of $\ln([MB]_0/[MB])$ with UV exposure time for different MB concentrations in the solution.....	47
FIGURE 4. 14 Variation in light absorption with UV exposure time for different MB concentrations in the solution	48
FIGURE 4. 15 Variation of percent MB concentration with UV exposure time for different MB concentrations in the solution	49
FIGURE 4. 16 Variation in light absorption with UV exposure time for different amounts of unreacted TiO ₂ in the solution	50
FIGURE 4. 17 Variation of percent MB concentration with UV exposure time for different amounts of unreacted TiO ₂ in the solution	50
FIGURE 4. 18 Variation of $\ln([MB]_0/[MB])$ with UV exposure time for different amounts of unreacted TiO ₂ in the solution	51
FIGURE 4. 19 Variation in light absorption with UV exposure time for different amounts of 3HAP-TiO ₂ in the solution.....	52
FIGURE 4. 20 Variation of percent MB concentration with UV exposure time for different amounts of 3HAP-TiO ₂ in the solution.....	53
FIGURE 4. 21 Variation of $\ln([MB]_0/[MB])$ with UV exposure time for different amounts of 3HAP-TiO ₂ in the solution.....	54

CHAPTER I

INTRODUCTION

Nowadays, more emphasis is given on the removal of undesired organic contaminants from air streams; or undesired organic compounds in water supplies and in the discharge of wastewater from chemical industries, power plants and agricultural sources [1,2]. In order to prevent the damages to environment, the use of photocatalyst to destroy organic compounds in contaminated air or water, or to convert them into harmless chemicals has been extensively studied for the last thirty-five years [3-5]. Titanium dioxide (TiO_2) is one of the most popular and promising photocatalyst for photocatalytic applications because of its high-availability, inexpensiveness, strong oxidizing power, high photostability, low toxicity and redox selectivity [5,6]. TiO_2 possesses biocompatibility and bioactivity, as well [7].

Because of the desirable features for the photocatalytic applications, the TiO_2 photocatalyst have been used for the purposes ranging from self-cleaning and air purification to water purification and bactericidal applications. Typical industrial applications of photocatalytic TiO_2 is shown in Figure 1.1. The photocatalytic oxidation for total organic carbon analysis, determination of dissolved organic nitrogen compounds in natural waters, water and air disinfection, removal of silver in photographic processing waste and photoreduction of mercuric salt solutions can also be exemplified as further environmental application of TiO_2 photocatalyst [8].

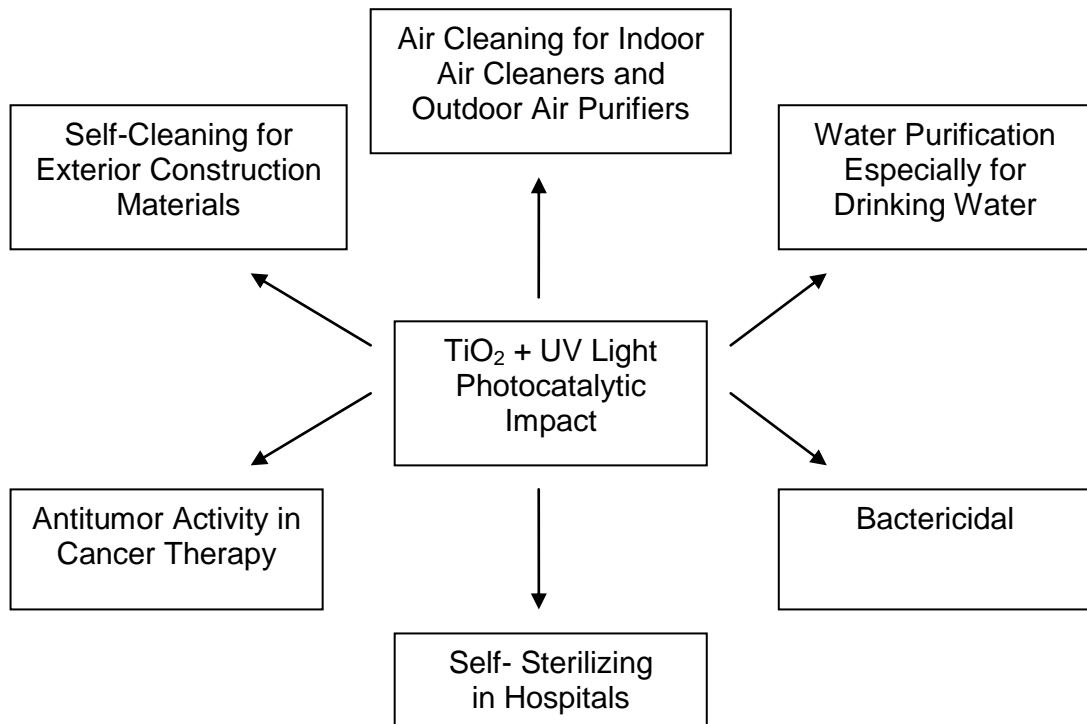


FIGURE 1. 1 Typical applications of photocatalytic TiO₂ [9]

TiO₂ is a wide band gap semiconductor ($E_g \approx 3.2$ eV for anatase). It has the highest photocatalytic detoxification efficiency. Furthermore, even light below 400 nm (i.e., 5% of the solar energy reaching the surface of the earth) is absorbed and capable of forming electron/hole pairs which are demanded for photocatalytic process. In other words, it is remarkable for the TiO₂ that the small near ultraviolet (UV) component of sunlight is sufficient to generate these electron/hole pairs on the ground level [3,5,10].

The industrial applications of TiO₂ however, are limited since TiO₂ photocatalyst can only decompose substances existing on or happened to be in contact with its surface. It has inability to attract substances to itself [11]. Also, direct application of TiO₂ on organic materials like organic paint, textile, plastics, and paper can lead to a degradation of the substrates, resulting in the delamination of the coating [12]. Both problems might be solved by apatite coating on the surface of TiO₂ [11,13]. Polluting components including bacteria, viruses, NO_x, ammonia and toxic chemical compounds are immediately absorbed by apatite, which then would allow reactive species of TiO₂ to decompose them upon UV exposure [12,13]. Therefore, if apatite and TiO₂ can be combined into a

composite with the attributes of both, the resulting product might be a good antibacterial and environmental purification material, having the ability to absorb and to decompose bacteria and other organic materials.

Kokubo et al. have introduced the biomimetic process of apatite-coating using Simulated Body Fluid (SBF) [14]. In this process a biologically active apatite layer is formed on a substrate after immersion in an artificially prepared supersaturated calcium and phosphate solution known as SBF [15]. SBF is prepared in accordance with the chemical analysis of human body fluid, with ion concentrations nearly equal to those of the inorganic constituents of human blood plasma [16]. Kasuga et al. reported that SBF could be successfully used to form apatite on TiO_2 [17].

Photocatalytic activity of photocatalytic materials can be measured by employing Methylene Blue (MB) test. MB is widely used as a standard target compound in a test of photocatalysts. MB might also be considered to be a model compound of organic pollutants because it is mixed into some fertilizers as a dye [18]. TiO_2 composites are reported to demonstrate exceptional performance in the photocatalytic degradation of MB [19]. Use of apatite coating may help to prevent TiO_2 from degrading the polymeric support material such as poly(methyl methacrylate) (PMMA).

The objectives of this study was to improve the photocatalytic activity of TiO_2 powders via apatite deposition on their surface through a biomimetic process and to investigate photocatalytic activity of apatite deposited TiO_2 powders on the photodegradation of PMMA. A series of experiments regarding the photocatalytic activity of apatite-deposited TiO_2 powder have been conducted by employing MB test in aqueous solution and by measuring the degradation of PMMA under UV irradiation.

CHAPTER II

LITERATURE REVIEW

2.1. PHOTOCATALYSIS

Environmental damage as a byproduct of technological growth is an increasing concern. More efforts have been given and new technologies have been developed for dealing with this problem. Photocatalysis allows in many cases a complete degradation of organic pollutants in very small and not noxious species, without using chemicals, avoiding sludge production and its disposal [20]. A wide spectrum of organic contaminants in water (for example, benzene and phenol, ketones, ethers, pesticides, chlorinated aliphatic, and aromatic compounds such as trichloroethylene and polychlorinated biphenyls, and other halogenated compounds) has been photocatalytically oxidized into nontoxic forms, such as simple mineral acids, carbon dioxide, and water [3,21]. Using photocatalysis for water and wastewater treatment, for instance, provides advantages such as degradation of color and odor compounds, destruction of disinfection byproduct precursors, and on-site treatment without the risk of transporting hazardous waste [3].

Since the discovery of photocatalysis by Fujishima and his co-workers in 1972, photocatalytic materials such as titanium dioxide (TiO_2), zinc oxide (ZnO), cadmium sulfide (CdS), and zinc sulfide (ZnS) have been widely studied [22]. These materials are defined as semiconductors that are activated by the absorption of a photon and help to accelerate a reaction, without being consumed [23]. Photocatalysis is a process that denotes an acceleration of

photoreaction in the case when there is a catalyst and light. Figure 2.1 illustrates the photocatalytic processes schematically. When a photocatalytic material is exposed to light, it absorbs photon energy and, as a result, various chemical reactions occur. The driving force of photocatalysis by semiconducting particles is the excess free energy of electron hole pairs generated in the particles by this light absorption [24].

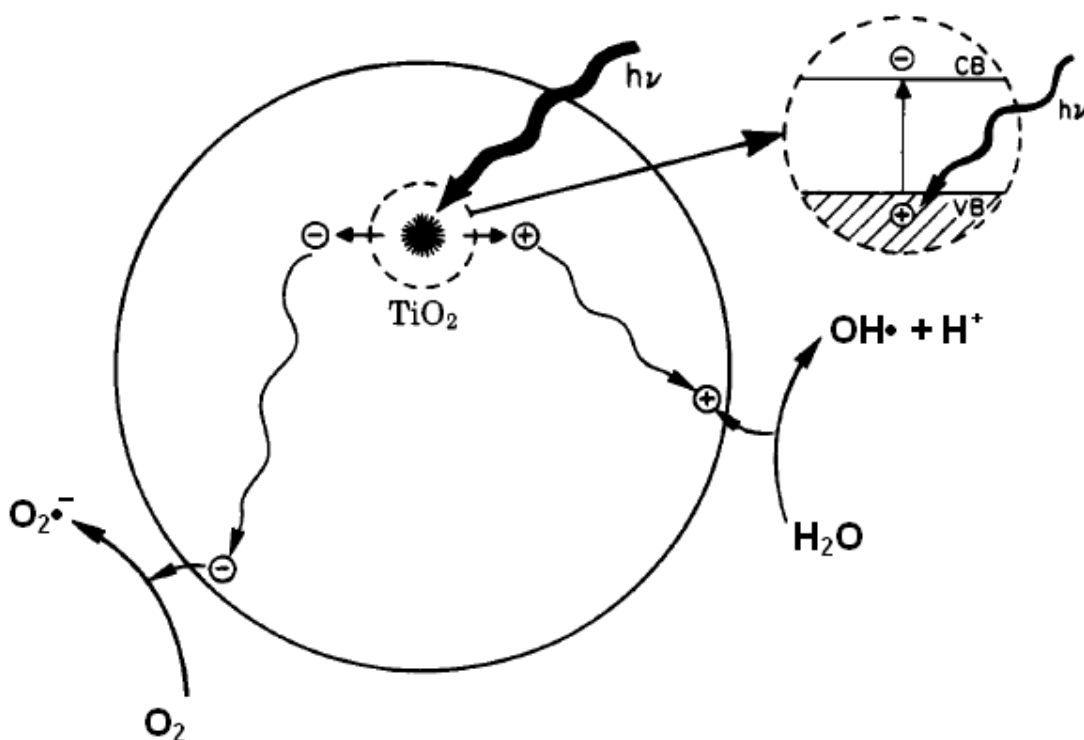
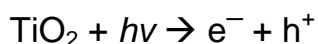


FIGURE 2. 1 Schematic illustration of photocatalytic events [24].

When a semiconductor is illuminated with photons of energy higher than or equal to its band gap, photoelectrons, e^- and photo-holes (or positions) h^+ are created [25]. If the semiconductor is immersed in water, for example, the holes react with water molecules (H_2O) or hydroxide ions (OH^-) and produce free hydroxyl radicals (OH^\bullet), very strong oxidants capable of oxidizing many organic compounds. Whereas OH^- has a charge of -1, the charge of OH^\bullet is zero; and OH^\bullet needs an electron in order to achieve stability. Although direct reactions of holes and organic molecules as well as other direct and indirect reactions may occur, hydroxyl radical oxidation is thought to be the primary mechanism for destruction of organic compounds [3,26]. The OH radicals oxidize hydrocarbons

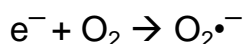
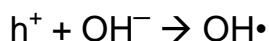
and other water insoluble organic compounds to water soluble ones: such as ketones, aldehydes, carboxylic acids, etc. and ultimately CO₂ [27,28]. The ultraviolet (UV) radiation used in photocatalysis may come from the sun or an artificial source. However, to generate electron hole pairs, the incident photons must have energy greater than the band gap of photocatalytic materials. Photocatalytic events consist of the following initial steps:

- 1- Electron/hole pair formation upon irradiation;

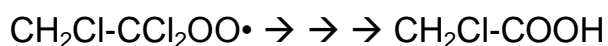
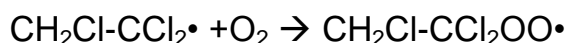
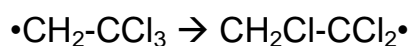


(where h is Planck's constant in units of J.s; ν is frequency in Hz; $h\nu$ is the formula for a photon energy in reactions; e^- is electron; h^+ is hole)

- 2- Formation of OH• and/or OOH• radicals and O₂•⁻ superoxide ions;



- 3- Attack of the surfactants by these activated radicals (for example, methylchloroform decomposes as in the following).



CH₂Cl-COOH (chloroacetic acid) decomposes into CO₂ and HCl [5,30-32].

Fujishima et al. [9] proposed a diagram of the processes occurring during photocatalytic oxidation of acetaldehyde (CH₃CHO) on an illuminated TiO₂ particle as seen in Figure 2.2.

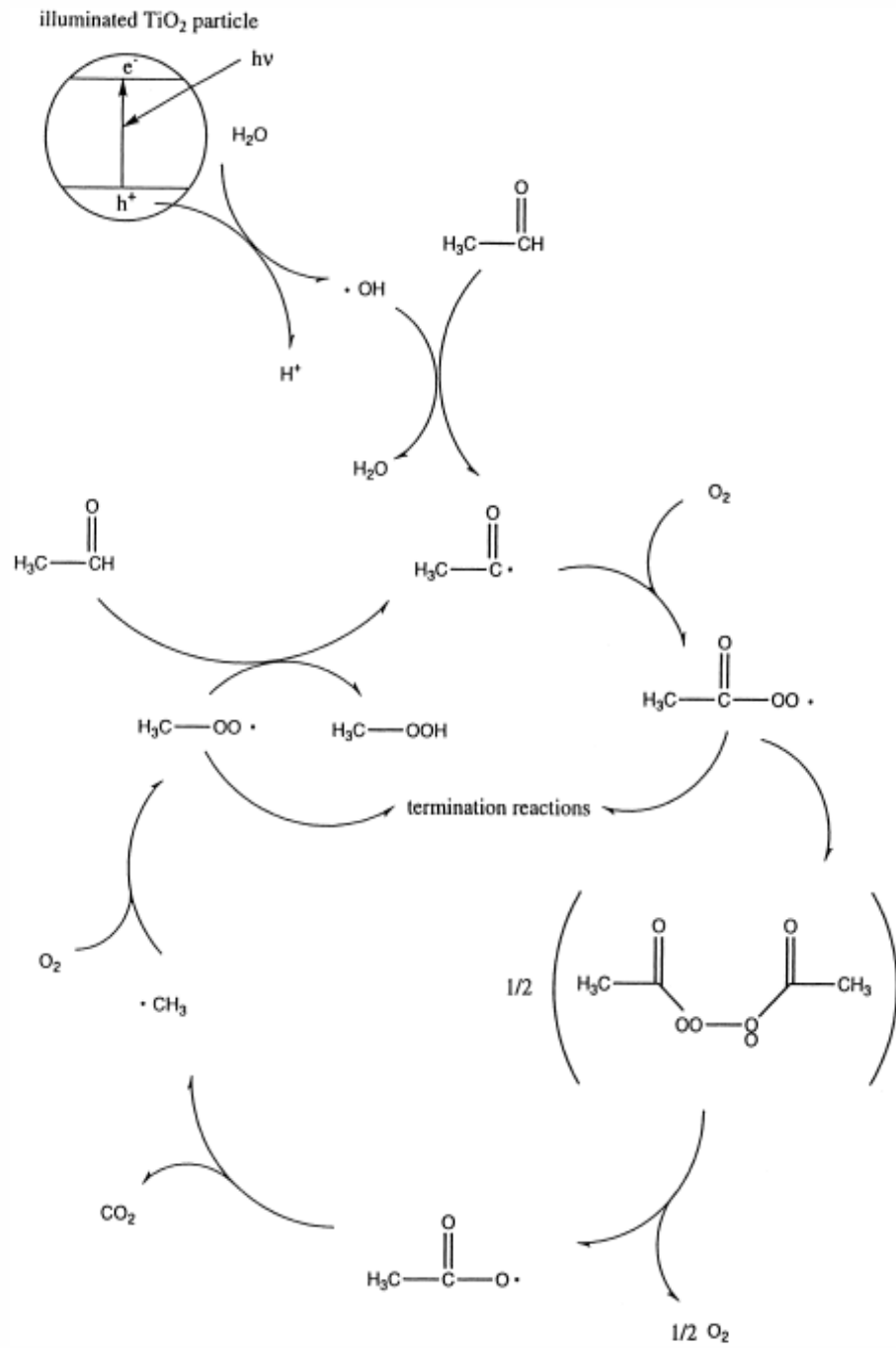


FIGURE 2. 2 Schematic illustration of the processes occurring during photocatalytic oxidation of CH_3CHO on an illuminated TiO_2 particle [9]

Factors influencing the photocatalyst activity include: structure and surface properties of the materials, particle size, preparation, spectral activation, resistance to mechanical stresses [23]. Among the possible advantages of using the photocatalysis technology, the following might be highlighted [33]:

- 1- a wide spectrum of organic compounds may be mineralized;
- 2- additional electron acceptors (such as H₂O₂) may not be required;
- 3- the photocatalyst may be reused; and
- 4- solar radiation may be employed as light source to activate the catalyst.

2.2. PHOTOCATALYTIC MATERIALS

Metal oxide semiconductors have been found to be the most suitable photocatalysts given their photocorrosion resistance and wide band gap energies [23]. Solid materials have two energy bands, called conduction band and valence band. Valence band represents the lower energy band filled with electrons, whereas conduction band represents the upper energy band being empty at absolute zero temperature. The band gap is referred to the energy difference between the top of the valence band and the bottom of the conduction band. When exposed to UV-light, the electrons are capable of bouncing up from the valence band to the conduction band, which generates electron hole pairs [34]. The band gaps and wavelengths of certain photocatalytic materials that are frequently used in academic studies are listed in Table 2.1.

TABLE 2. 1 Selected photocatalytic materials, their band gaps and wavelengths [35]

Photocatalytic Material	Band Gap (eV)	Wavelength (λ-nm)
TiO ₂ (anatase)	3.2	388
TiO ₂ (rutile)	3.0	413
SnO ₂	3.6	338
ZnO	3.4	363
Fe ₂ O ₃	2.3	539

2.2.1. Photocatalytic Titanium Dioxide (TiO₂)

Combining properties of optical transparency, non-toxicity, ease of fabrication, chemical stability and high surface area, TiO₂ is one of the most active photocatalysts [6,7]. Recently, fairly intensive studies have been done on light-induced mineralization of organic pollutants with the use of TiO₂ photocatalyst to develop a new technology for air and water remediation. Through its strong oxidative capabilities, TiO₂ is regarded as a promising material for the treatment of gas and liquid pollutants such as nitric oxide (NO), volatile organic compounds, hydrogen nitrate (HNO₃), ammonia (NH₃), and compounds containing sulfur [19]. Ollis et al. [35] showed that in the presence of near-UV illuminated TiO₂; common chlorinated aliphatic hydrocarbon contaminants in water, were not only dechlorinated but completely mineralized. Furthermore, it was also reported that under similar conditions not only chlorinated aliphatic compounds, but a whole range of contaminants, including some aromatic compounds that are resistant to oxidation were converted to carbon dioxide [36,37].

TiO₂ occurs in three different crystal structures (rutile, anatase, and brookite), among which anatase is reported to be the most efficient photocatalyst during chemical reactions. The reason is that anatase shows better adsorptive affinity and higher band gap value than those of rutile [38]. TiO₂ shows relatively high reactivity and chemical stability under UV light [wavelength (λ) < 385 nm], whose energy exceeds the band gap (the minimum amount of energy required for exciting the electron) of 3.2 eV in the anatase crystalline phase [10,27,33]. Therefore, the 300 to 387.5 nm portion of solar insolation available on the ground level might be used with this photocatalyst [3]. Under this information, it should be asserted that when UV is illuminated onto TiO₂, the photon energy generates an electron hole pair on the TiO₂ surface. The hole in the valence band can react with H₂O or hydroxide ions adsorbed on the surface to produce very active hydroxyl radicals (OH•), and the electron in the conduction band can reduce O₂ to produce super-oxide ions (O₂•-). Both holes and (OH•) are extremely reactive upon contact with organic compounds [4,5,26]. Moreover,

whether the oxidation of organic compounds is through various radical groups in solution or through direct hole oxidation on catalyst surface depends on the substrates presented in solution and reaction conditions [30,39].

2.3. ENHANCEMENT of PHOTOCATALYTIC ACTIVITY of TiO₂

Various attempts have been made to improve photocatalytic activity of TiO₂. One of the attempts involves an increase in the surface density of hydroxyl and oxygen molecules so that it will result in better adsorption of electron hole pairs [35]. Another attempt is to increase the surface area of the photocatalytic material. A highly porous surface structure is very effective because it offers a much larger number of catalytic sites than a dense surface [40]. The same logic would also apply if a smaller particle size is to be used. Although high surface area enhances the photocatalytic activity, it also causes instability of particles. For instance, structure of nanoparticles can be damaged because of the environmental factors including temperature, pressure, existence of fluids, etc [35]. The third attempt involves the dopant effect. For instance, Nd³⁺- and Pd²⁺-doped TiO₂ provides better photocatalytic activity [38]. Much attention has been paid to doping with transition metals and noble metals. However, metal doping can also cause photocatalytic activity to disappear in case of large metal particles. Since metal particles become charge adsorption centers, they should be well dispersed on the surface [35].

The fourth way for increasing the photocatalytic activity is the apatite coating on TiO₂. Since TiO₂ lacks to attract substances, it can only decompose the substances that happened to come into contact. On the other hand, apatite, which possesses a photocatalytic property itself, has an ability of absorbing bacteria and organic substances, such as protein and pollen, with or without the light exposure. Thus, coating photocatalytic TiO₂ with apatite can result in decomposition of more organic substances, viruses, and bacteria. Another

advantage of the apatite coating method can also be realized as it prevents the support material to be decomposed by the TiO_2 [11].

2.4. APATITE DEPOSITION and SIMULATED BODY FLUID

The TiO_2 eliminates odors, microbes and moulds by decomposing them into carbon dioxide, water and other small molecules. However, the uses of TiO_2 are limited since decomposition occurs only for substances with which it happens to come into contact. On the other hand, Hydroxyapatite (HAP), which is an insoluble calcium phosphate mineral of composition $\text{Ca}_{10}(\text{PO}_4)_6(\text{OH})_2$, has been used as a cation exchanger and adsorbent in wastewater treatment, and it has a very high capacity for removing divalent heavy metal ions from water and liquid waste [41,42]. HAP, hereafter will be referred to as apatite, is known not only as a primary constituent of the biological hard tissues, but also as adsorbents and catalysts. The surface OH^- groups absorb CO_2 , NO_x , H_2O and organic compounds; and have excellent affinity to biomaterials such as proteins. Positively charged proteins interact nonspecifically with the general negative charge on the apatite produced by immobilized phosphate ions. In the case of negatively charged proteins, interaction is a balance between electrostatic repulsion by the negative charge on the apatite and specific complexation between protein carboxylic acid groups and apatite calcium sites [42-44]. The ionic ratio of Calcium (Ca) to Phosphate (P) is ideally $10/6=1.67$ [45,46].

Photocatalytic reactions of organic compounds, such as alcohol, 1-butene, and cyclohexanone oxime, and chlorobenzene on apatite are known. Nishikawa [47] reported on the activation of stoichiometric apatite by UV irradiation and on the formation of radical species, such as O_3^- from UV irradiation. The photocatalytic behavior of apatite would also be due to the formation of $\text{O}_2^{\bullet-}$ by UV irradiation. It should also be noted that the active hydroxyl and oxygen radicals, OH^\bullet and $\text{O}_2^{\bullet-}$, might be efficiently generated on apatite by photo-induced excitation with UV irradiation in case where the surrounding molecule, H_2O or O_2 , are as well

present. In detail, $O_2^{\bullet-}$ would be generated by electron transfer to O_2 after the photo-induced excitation, and OH^\bullet would be produced by the reaction of $O_2^{\bullet-}$ and H_2O .



These radicals must cause the decomposition of organic pollutants as similar to TiO_2 photocatalyst [48,49].

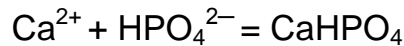
The combination of TiO_2 and apatite might be expected to result in the attraction and absorption of the chemical pollutants by the apatite on the surface, and decomposition of them by the TiO_2 under UV light. Apatite coating is widely and successfully conducted through plasma spray method. The plasma sprayed apatite coatings are indeed produced in a short time and the coating–substrate adhesion is strong. However, this method is not only relatively expensive; but also, the structure and phase composition of the plasma sprayed coatings are different from those of the natural bone and are difficult to be controlled at high temperatures [50].

Apatite powders have been synthesized from aqueous solutions for use in bioceramic applications [15]. The formation of the apatite layer can also be reproduced on the surface of bioactive materials in an acellular SBF [51]. SBF has the chemical analysis of human body fluid with ion concentrations nearly equal to those of the inorganic constituents of human blood plasma, and it is mainly utilized to prove the similarity between in vitro and in vivo behavior of certain glass-ceramic compositions and to eliminate the melting problem occurred due to the plasma spray method [52,53]. Besides, since Ca-P precipitation in SBF is similar to biological mineralization, the use of SBF might provide an alternative method of creating Ca-P coatings [54]. Ion concentration of SBF in comparison with human blood plasma is given in Table 2.2.

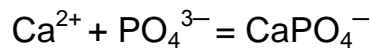
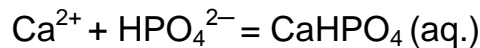
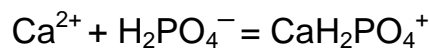
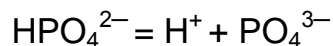
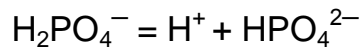
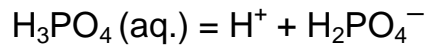
TABLE 2. 2 Ion concentration in SBF and human blood plasma [54]

	Concentration (mM)							
	Na ⁺	K ⁺	Mg ²⁺	Ca ²⁺	Cl ⁻	HCO ₃ ⁻	HPO ₄ ²⁻	SO ₄ ²⁻
SBF	142.0	5.0	1.5	2.5	147.8	4.2	1.0	0.5
Human Blood Plasma	142.0	5.0	1.5	2.5	103.0	27.0	1.0	0.5

The SBF solution introduced in Table 2.2 belongs to the original SBF (1-SBF). It is possible to diversify the kinds of SBF solutions. For instance, Bayraktar and Tas [52], and Lu and Leng [54] have used different kinds of SBF by modifying the ion concentration in the original SBF recipe. Dicalcium phosphate (CaHPO₄·2H₂O), octacalcium phosphate (Ca₈(HPO₄)₂(PO₄)₄·5H₂O) or apatite are among the precipitated Ca-P phases in aqueous solutions. HAP is regarded as the most thermodynamically stable material among these three in physiological environments. The reaction for precipitation in aqueous solutions defining the ion units of apatite is given below [54].



Other significant reactions in SBF might be given as follows [54-56]:



Biomimetic deposition processes last about 7–14 days with daily refreshments. Two possible ways have been recommended to shorten this period. First, some chemical treatments could reduce soaking time and enhance calcium phosphate deposition. However, these surface treatments might weaken the calcium phosphate/substrate interface. Second, increasing SBF concentration with

respect to Ca and P ions (e.g., using 1.5-SBF; 4-SBF; 10-SBF) could also shorten immersion time [15,57,58].

Figure 2.3 shows the schematic diagram of the mechanism of apatite formation on the TiO_2 coatings in SBF. The surface of the TiO_2 is negatively charged (OH^-). This negative surface provides favorable sites for calcium phosphate nucleation. The Ca^{2+} and PO_4^{3-} ions will be assembled on the surface of TiO_2 to form apatite [59].

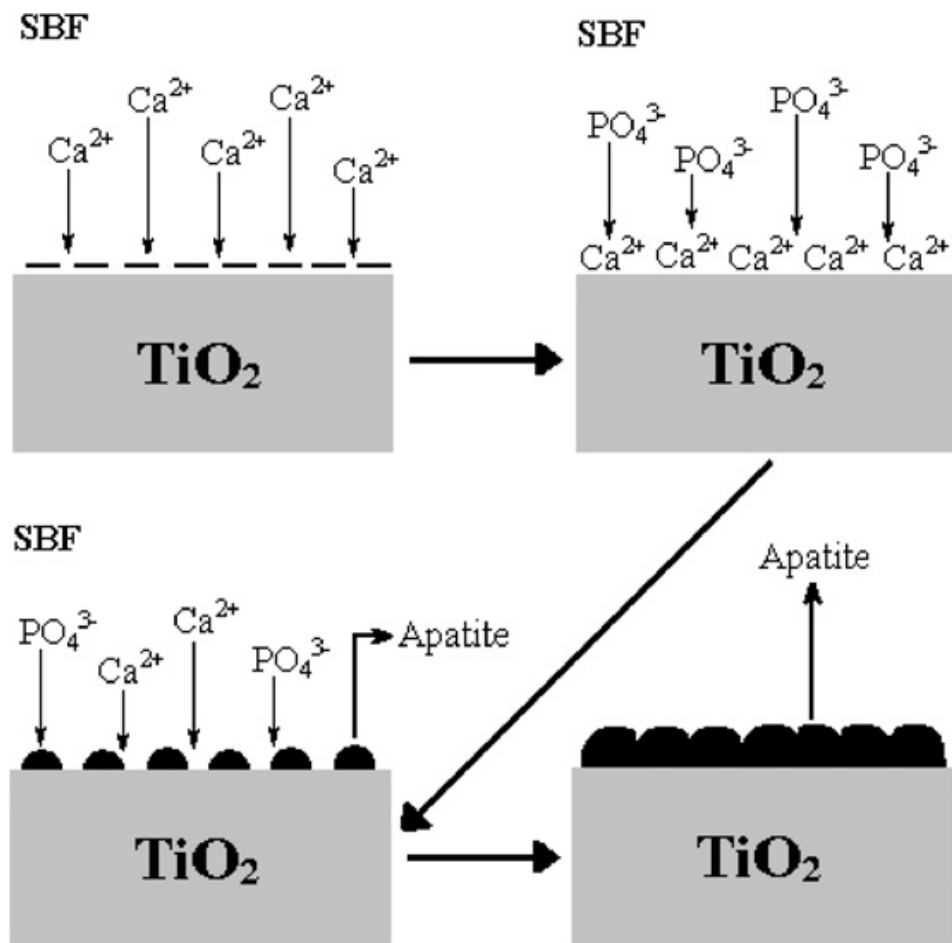


FIGURE 2. 3 Schematic diagram showing the mechanism of apatite formation on TiO_2 coating in SBF [59]

2.5. METHYLENE BLUE (MB)

MB is a brightly colored blue cationic thiazine dye, with maximum wavelength values at 664 and 292 nm. MB can be used as an antidote for cyanide poisoning in humans, antiseptic in veterinary medicine and, most commonly, in vitro diagnostic in biology, cytology, hematology and histology [60]. Figure 2.4 illustrates the structure of MB.

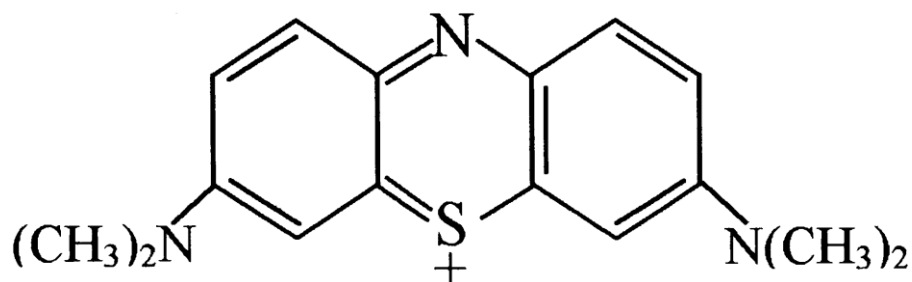


FIGURE 2. 4 The structure of Methylene Blue [60]

MB is widely used as a standard target compound for investigating photocatalytic activity of photocatalysts. Mills and Wang [60] have reported that MB was photoreduced to its colourless *leuco* form, LMB, by the TiO_2 photocatalyst. MB can also be regarded as a model compound of organic pollutants because it is mixed into some fertilizers as a dye [18]. The use of MB in photocatalytic investigations has several advantages as listed below [60,61]:

- 1- It is a well defined optical absorption maximum at 664 nm, where light scattering is minimized,
- 2- It is good resistance to light degradation in the absence of photocatalyst,
- 3- It is optically transparent at the wavelength range studied (320 nm to 380 nm),
- 4- It is a common dye whose bleaching might be followed easily using spectro-photometric techniques.

The photocatalytic degradation of several materials, including MB in the presence of TiO₂, obeys Langmuir-Hinshelwood kinetic model, described by the following equation:

$$r = -\frac{d[MB]}{dt} = \frac{kK[MB]}{1 + K[MB]}$$

where r is the rate of reaction that changes with time, k is the rate constant, K is the adsorption constant, and t is time.

This equation can be integrated between the limits: [MB] = [MB]₀ at t = 0, and [MB] = [MB] at t = t. The following equation gives this integration.

$$\ln\left(\frac{[MB]_0}{[MB]}\right) + K([MB]_0 - [MB]) = kKt$$

This equation represents the exact solution for the degradation of MB. However, if the concentration of MB is in the scale of milimoles; i.e., if K[MB] << 1, an apparent first-order model can be realized as follows:

$$r = kK[MB]$$

Integrating this equation with respect to limits: [MB] = [MB]₀ at t = 0, and [MB] = [MB] at t = t, the result will become:

$$\ln\left(\frac{[MB]_0}{[MB]}\right) = K_{ap}t$$

where K_{ap} (=kK) is the apparent reaction rate constant [62,63].

2.6. POLY (METHYLMETHACRYLATE) (PMMA)

PMMA, also known as paramethoxymethamphetamine or *N*-methyl-1-(4-methoxyphenyl)-2-aminopropane, is a structural hybrid of two phenylisopropylamine stimulants: PMA (or paramethoxyamphetamine) and methamphetamine. [64]. Figure 2.5 illustrates the structures of PMMA, PMA and methamphetamine.

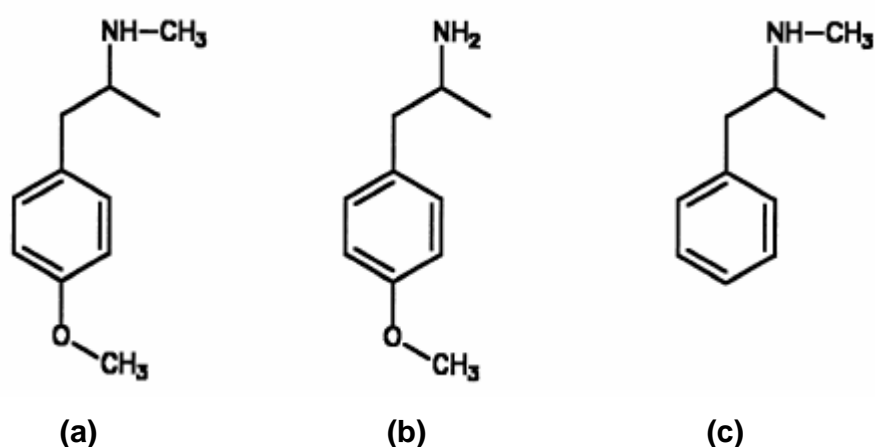


FIGURE 2. 5 Structures of (a) PMMA, (b) PMA, and (c) methamphetamine [64]

Although the strong oxidizing activities of TiO₂ contribute to several applications, the separation of TiO₂ powders from the suspension after treatment is problematic. In order to solve this problem, supported photocatalysts have been developed; in particular, TiO₂ powders has been immobilized on supports transparent to UV radiation [12,65]. Iketani et al. [66] have prepared TiO₂/poly(dimethylsiloxane) hybrid with sol-gel method and spin-coated on PMMA where PMMA is used as a support material. In a similar way, photocatalytic reactors are also made of UV transparent PMMA [67]. This, however, causes another problem. Although PMMA cannot extensively react with O₂, it reacts with the radical oxygen species generated during the TiO₂ photocatalytic reaction, such as HO• or hydroperoxyl radical (HO₂•) [68]. Direct application of TiO₂ on organic materials like plastics can lead to a degradation of the substrates, resulting in the delamination of the coating. A similar

photochemical decomposition effect was also found with organic paint, textile, plastics, and paper. Therefore, one of the key subjects that have to be solved in the case of an organic substrate is how to protect the substrate from degradation. In order to alleviate this problem Nonami et al. have proposed the use of TiO_2 covered with apatite applied for environmental purification [11].

CHAPTER III

EXPERIMENTAL PROCEDURE

3.1. PROPERTIES of TITANIUM DIOXIDE (TiO₂)

TiO₂ powders used throughout this study were commercially available and obtained from Nano Co. They had a purity better than 98.7 weight percentage (wt%) and were used without further purification. The chemical and physical properties of TiO₂ powders are listed in Table 3.1.

TABLE 3. 1 Chemical and physical properties of TiO₂ [69]

Property	Value
Crystallinity	Anatase
TiO ₂ content (wt%)	> 98.7
Impurity	SO ₃ : 0.454 Fe ₂ O ₃ : 0.032 K ₂ O : 0.121 Nb ₂ O ₅ : 0.290 P ₂ O ₅ : 0.122 Al ₂ O ₃ : 0.009 SiO ₂ : 0.013
Particle Size (μm)	1 ~ 1.5
Specific Surface Area (m ² /g)	101.5
Apparent Density (g/cc)	0.30 ~ 0.35

3.2. PREPARATION of SIMULATED BODY FLUID (SBF)

A SBF solution which had calcium and phosphate ion concentrations 10 times greater than those of human blood plasma was prepared and used as an incubation solution for apatite formation on the surface of TiO₂ powders. Hereafter this SBF is named 10-SBF and used throughout this thesis unless otherwise is mentioned. Table 3.2 presents the ion concentrations in human blood plasma, SBF and 10-SBF. The 10-SBF solution could be used for apatite coating on TiO₂ [7,13,17].

TABLE 3. 2 Ion Concentrations in human blood plasma, SBF and 10-SBF [70]

Solution	Ion Concentration (mmol/l)							
	Na ⁺	K ⁺	Mg ²⁺	Ca ²⁺	Cl ⁻	HCO ₃ ⁻	HPO ₄ ²⁻	SO ₄ ²⁻
Human Blood								
Plasma	142.0	5.0	1.5	2.5	103.0	27.0	1.0	0.5
SBF	142.0	5.0	1.5	2.5	147.8	4.2	1.0	0.5
10-SBF	1025.6	5.0	5.0	25.0	1064.0	10.0	8.3	0.5

The 10-SBF solution was prepared by dissolving appropriate quantities of NaCl, KCl, CaCl₂·2H₂O, MgCl₂·6H₂O, NaH₂PO₄ and NaHCO₃ in distilled water. All of the reagents were analytical grade and supplied from Merck Co. The starting materials were carefully weighed (\pm 0.0001 g) to their proper amount in an analytical balance (Mettler Toledo). A certain amount of NaHCO₃ was added into the solution in order to adjust the pH to a value in the range of 7.25 to 7.40. The reagents used for preparing 10-SBF and their weight percentages are given in Table 3.3.

TABLE 3. 3 Weight percentages of reagents used for preparing 10-SBF

Reagent	Weight percentage
NaCl	89.2
KCl	0.6
CaCl ₂ . 2H ₂ O	5.7
MgCl ₂ . 6H ₂ O	1.5
Na ₂ HPO ₄ . 2H ₂ O	1.8
NaHCO ₃	1.2

The reagents were added one by one after each one of the reagent was completely dissolved in distilled water at room temperature to avoid any unexpected chemical reactions among them. In order to obtain the chemical homogeneity, the SBF solution was stirred with a magnetic stirrer for about 15 min. After stirring is complete, a pH meter (HANNA) was employed to measure the pH value of the solution. All these processes were conducted under the ambient laboratory conditions. All the beakers and appliances used in the processes were cleansed with dilute hydrochloric acid solution. De-ionized water was used as sterilizing agent.

3.3. APATITE DEPOSITION on TiO₂ POWDERS

In order to form apatite on TiO₂ powders, a 1.5 g of TiO₂ powder was immersed into 300 ml of the 10-SBF solution at 37 °C for 1, 3, 6, 12, and 24 h. The solution containing TiO₂ powders was stirred continuously at a rate of 200 rpm through the entire immersion duration by using a magnetic stirrer. Upon completing the immersion duration, the solution was filtered by using a filter paper (Whatman Inc.) to acquire TiO₂ powders. The mesh size of the filter paper was 35 µm maximum. Acquired TiO₂ powders were washed using de-ionized water, and were filtered again. After that, the powders were left in an oven at 60 °C for a

day to achieve complete drying. Finally, the dried powders were pounded in order to avoid agglomeration.

The flowchart for the experimental procedure for the apatite deposition on TiO_2 powders is shown Figure 3.1.

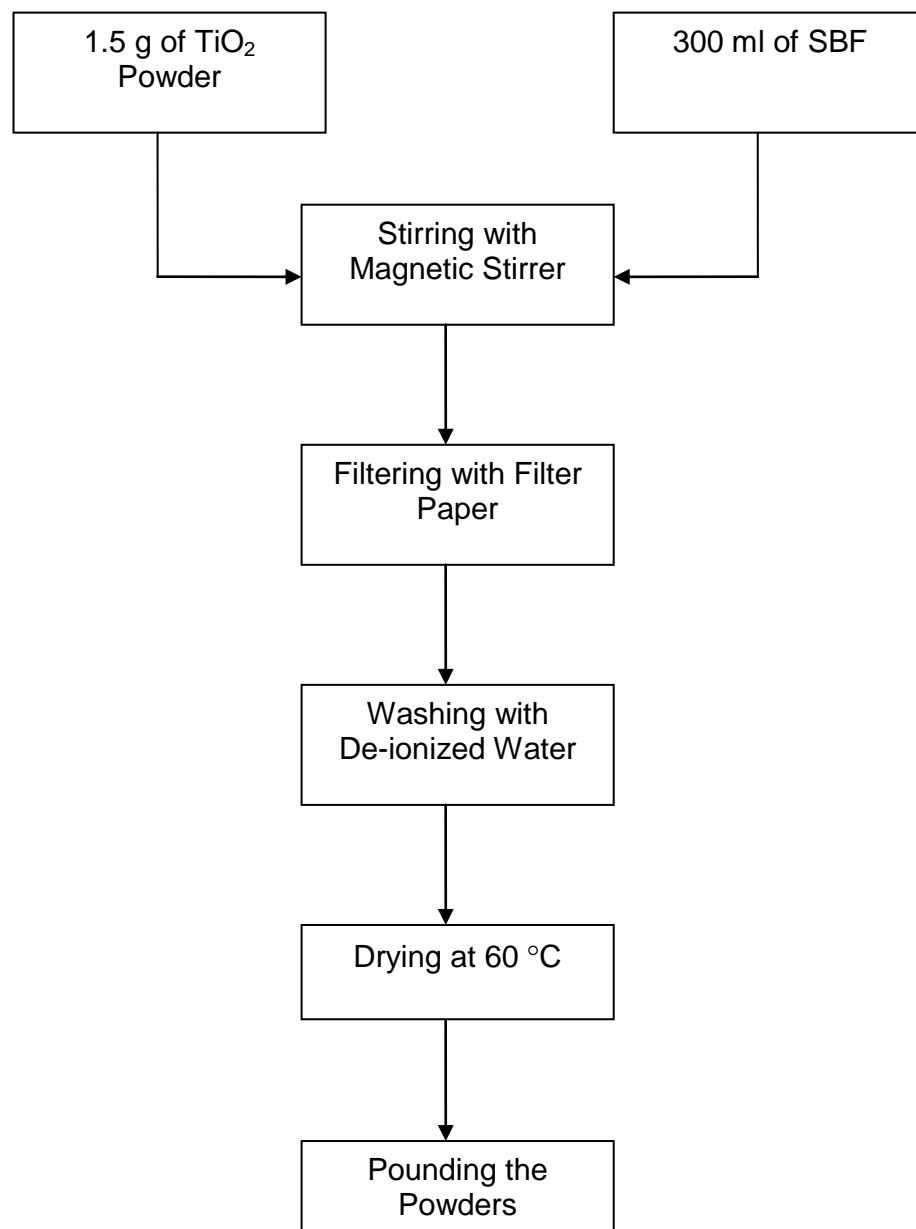


FIGURE 3. 1 Flowchart showing the experimental procedure for apatite deposition on TiO_2 powders

3.4. PREPARATION of the COMPACTS of PMMA and TiO₂ POWDERS

10 g of PMMA and 0.5 g of unreacted or apatite deposited TiO₂ powders were mixed in a mortar with pestle. The mixtures were hot pressed at 180 °C to form compacts by using a mounting press machine (Struers Co.). A pressure maximum of 30 kN was applied for 15 min; the first 8 min of which was devoted to heating up to 180 °C and the rest 7 min to cooling down to room temperature. The compacts were then surface polished using P240A grade abrasive papers. The flowchart of the experimental procedure for the preparation of the compacts composed of PMMA and TiO₂ powder is shown in Figure 3.2.

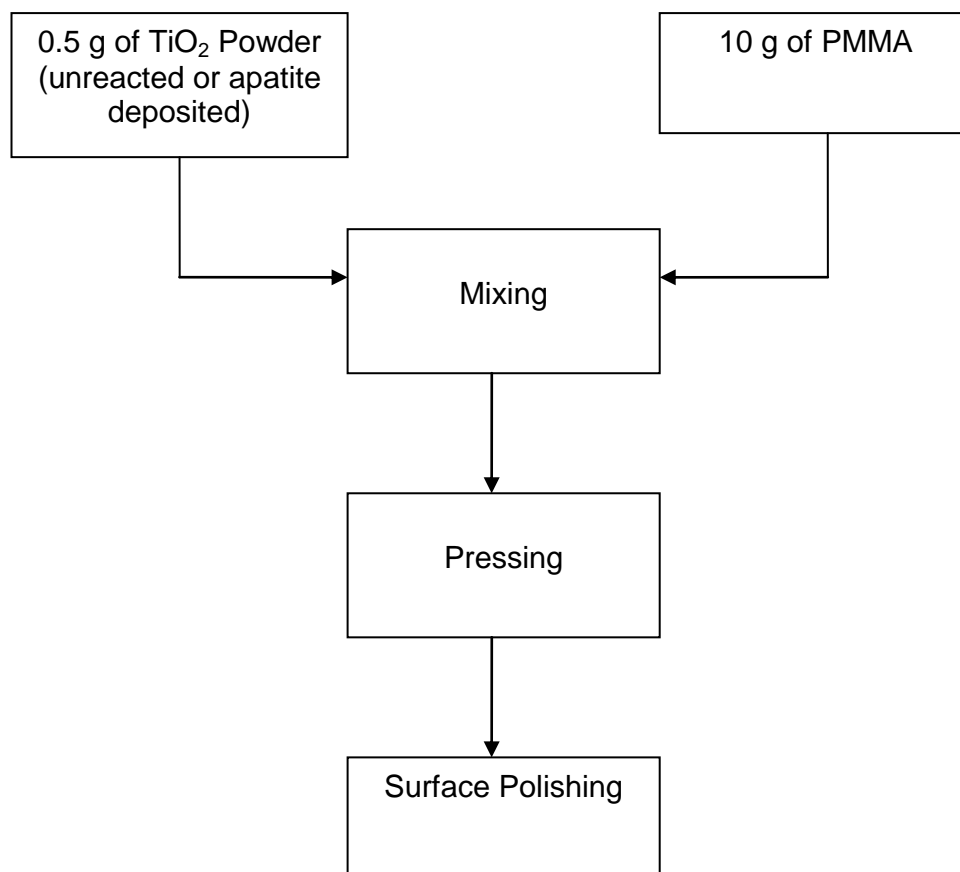


FIGURE 3. 2 Flowchart showing the experimental procedure for the preparation of the compacts composed of PMMA and TiO₂ powders

3.5. CHARACTERIZATION

3.5.1. X-Ray Diffraction (XRD) and Fourier Transform Infrared Spectroscopy (FTIR) Analyses

Powder XRD was employed to identify phases formed on the surface of TiO₂ powders during immersing in 10-SBF. The XRD patterns of bare TiO₂ powders and the TiO₂ powders immersed in the 10-SBF solution for various durations (1, 3, 6, 12, and 24 h) were taken by using a Rigaku Geiger-Flex DMAX/B model diffractometer with Ni-filtered CuK_α radiation. Each sample was scanned from 2θ of 20° to 50° at a rate of 2°/min by 0.02° increments continuously.

Structural analyses of the TiO₂ powders were done by Fourier transform infrared spectroscopy, FTIR, (Bruker IFS 66/S, FRA 106/S) before and after immersion in 10×SBF. The spectrum was measured from wavenumber 4000 to 400 cm⁻¹.

3.5.2. Scanning Electron Microscope (SEM) and Energy Dispersive Spectroscopy (EDS) Analyses

A SEM (JSM-6400, Jeol) was employed to examine the surface morphology of the TiO₂ powders and the TiO₂ powders immersed in the 10-SBF solution for different durations (i.e., 1, 3, 6, 12, and 24 h). The representative electron micrographs were taken for the evidence of apatite formation on the surface of TiO₂ powders. Before the SEM analyses, a thin layer of Au was coated onto samples. Elemental analysis of the samples was performed using EDS (Noran Instruments Co).

3.6. PHOTOCATALYTIC ACTIVITY MEASUREMENTS

The photocatalytic activity of the TiO₂ powders immersed in the 10-SBF solution for different durations and of the compacts composed of PMMA and TiO₂ powder mixtures was measured inside a homemade box which did not allow light exposure inside and was virtually isolated from the external factors. Inside the box, there were a Black-Ray-grade UV semiconductor inspection lamp (100 Watt, 230V~50Hz, 2.0 Amp, 365 nm), a magnetic stirrer, and a Pyrex glass vessel surrounded by a circulating water jacket to cool the reacting solution.

3.6.1. Photocatalytic Activity of the Compacts of PMMA and TiO₂ Powders

Photocatalytic activities of the compacts composed of PMMA and TiO₂ powders immersed in the 10-SBF solution for different durations were determined by measuring the weight loss of the samples under UV light. The compacts were placed in the dark box and the UV light was turned on. The weight change of compacts with respect to UV exposure time was monitored in every 30 min. The accuracy of the weight measurements was ± 0.0001 g of the data taken. Percent weight change in compacts with increasing UV exposure time was calculated by the formula;

$$\text{Percent Weight Change} = ((W_0 - W_t) / W_0) \times 100$$

where: W_0 is the initial weight of the compact and W_t is the weight of the compact at time t. The whole measurement process took 360 min. The flowchart for the measurement of the photocatalytic activity of the compacts composed of PMMA and TiO₂ powder is shown in Figure 3.3.

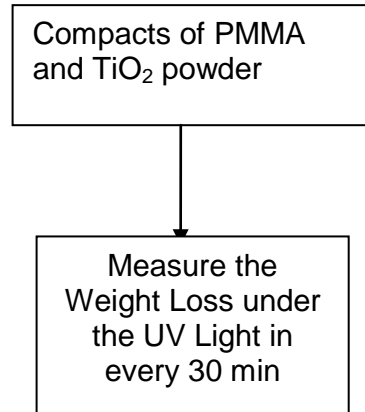


FIGURE 3. 3 Flowchart showing the experimental procedure for the measurement of the photocatalytic activity of the compacts composed of PMMA and TiO₂ powders

3.6.2. Photocatalytic Activity of TiO₂ Powders in Methylene Blue (MB) Solution

Photocatalytic activity of the TiO₂ powders immersed in the 10-SBF solution for different durations was determined using an aqueous MB solution that was prepared by dissolving 0.01 g of MB powder (Fluka) in 1 l of de-ionized water. This process resulted in preparation of an aqueous solution containing 10 mg/l of MB. A 300 ml of the MB solution prepared and 0.3 g of TiO₂ powder were mixed to obtain a suspension that was transferred immediately to the vessel in the box-built. In the vessel the suspension was stirred continuously at constant stirring rate of 500 rpm by a magnetic stirrer. In order to prevent the light-induced heat, the vessel was cooled with a water-cooling system during the entire test duration. In the first 30 min of the experiment, the UV light was not turned on in order for the TiO₂ powders to absorb the MB solution and to establish absorption-desorption equilibrium. At the end of 30 min, a sample was taken from the suspension by using Millipore syringes (pore size 0.22 μm), and Millex syringe driven filter units. The light-absorption spectra of the suspension was then measured under the UV light by using a spectrophotometer (Optima, SP-300) at the wavelength of 664 nm. After the first 30 min in the dark, the UV light was switched on. Afterwards, the change of absorbance intensity with UV

irradiation time was monitored in every 30 min. These measurements continued until the light-absorption value of 0.037 (the value for de-ionized water) was reached. These processes took between 1 to 4 h depending on the apatite deposition on the TiO₂ powder. Percent concentration change in MB solution with increasing UV exposure time was calculated by the formula;

$$\text{Percent concentration change} = \frac{LA_0 - 0.037}{LA_0 - 0.037} \left(\frac{LA_t - 0.037}{LA_0 - 0.037} \right) \times 100$$

where LA₀ is the initial light absorption value and LA_t is the light absorption value at time t.

The flowchart for the measurement of the photocatalytic activity of TiO₂ powders immersed in the 10-SBF solution for different durations is shown in Figure 3.4.

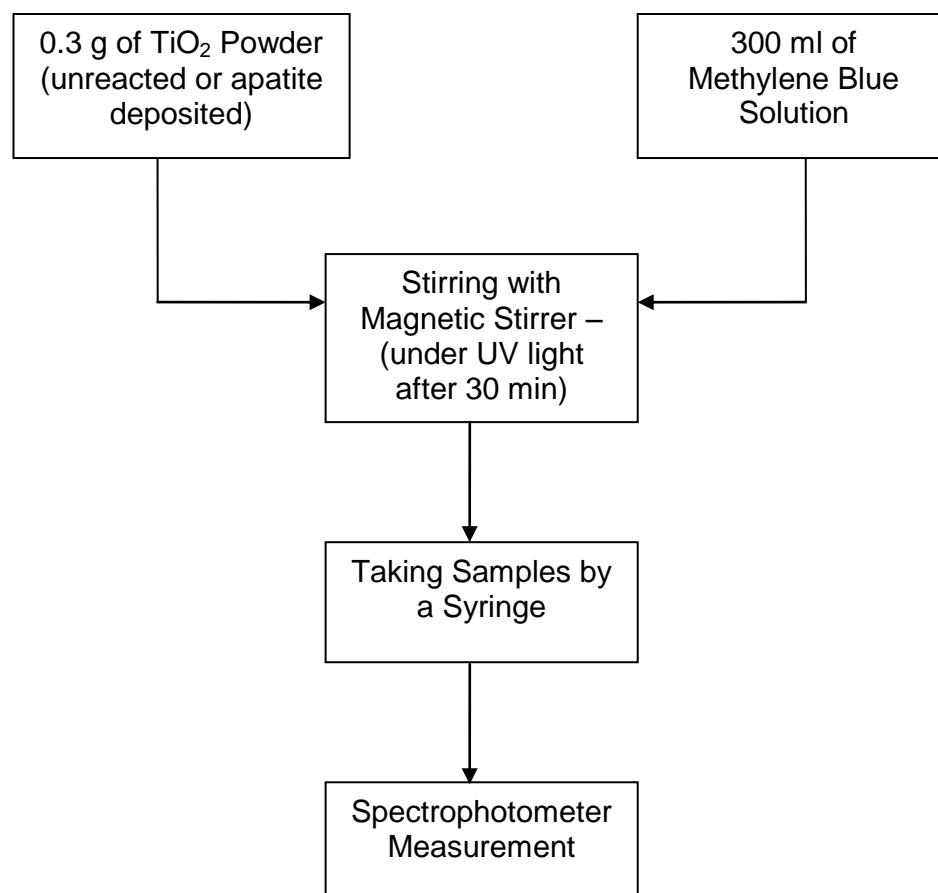


FIGURE 3. 4 Flowchart showing the experimental procedure for the measurement of the photocatalytic activity of the TiO₂ powders in the MB solution

In order to understand the effects of TiO₂ powder concentrations on the photocatalytic decomposition, different suspensions were prepared by keeping the amount of the aqueous MB solution constant (10 mg/l) but by changing the amount of TiO₂ powder. For that purpose, 0.3, 0.6, and 1.0 g of TiO₂ powder was loaded in the MB solution. These experiments were carried out only for bare TiO₂ powders and for the TiO₂ powders immersed in the 10-SBF solution for 3 h.

In order to see the effects of initial MB concentration in the aqueous solution on the photocatalytic decomposition of TiO₂ powders, different suspensions were prepared by keeping the amount of TiO₂ powder constant (0.3 g) but by changing the concentration of aqueous MB solution. For that purpose, MB concentrations of 2.5, 5, and 10 mg/l were used. These experiments were carried out only for bare TiO₂ powders and the TiO₂ powders immersed in the 10-SBF solution for 3 h.

CHAPTER IV

RESULTS AND DISCUSSION

4.1. GENERAL

In this chapter, data obtained from the conducted experiments are presented and the results are discussed.

The bare TiO₂ powders and the TiO₂ powders immersed in the 10-SBF solution for 1, 3, 6, 12, and 24 h durations are hereafter named unreacted TiO₂, 1HAP-TiO₂, 3HAP-TiO₂, 6HAP-TiO₂, 12HAP-TiO₂, and 24HAP-TiO₂, respectively, with regard to the immersion durations 10-SBF.

4.2. CHARACTERIZATION

4.2.1. X-Ray Diffraction (XRD) and Fourier Transform Infrared Spectroscopy (FTIR)

The XRD patterns of TiO₂ powders obtained before and after immersion in 10-SBF for different durations are given in Figure 4.1. The patterns indicate the characteristic (101) diffraction peak of anatase TiO₂ at 2θ of ~25.3° before and after immersion of the powders in 10×SBF, JCPDS card # 89-4921.

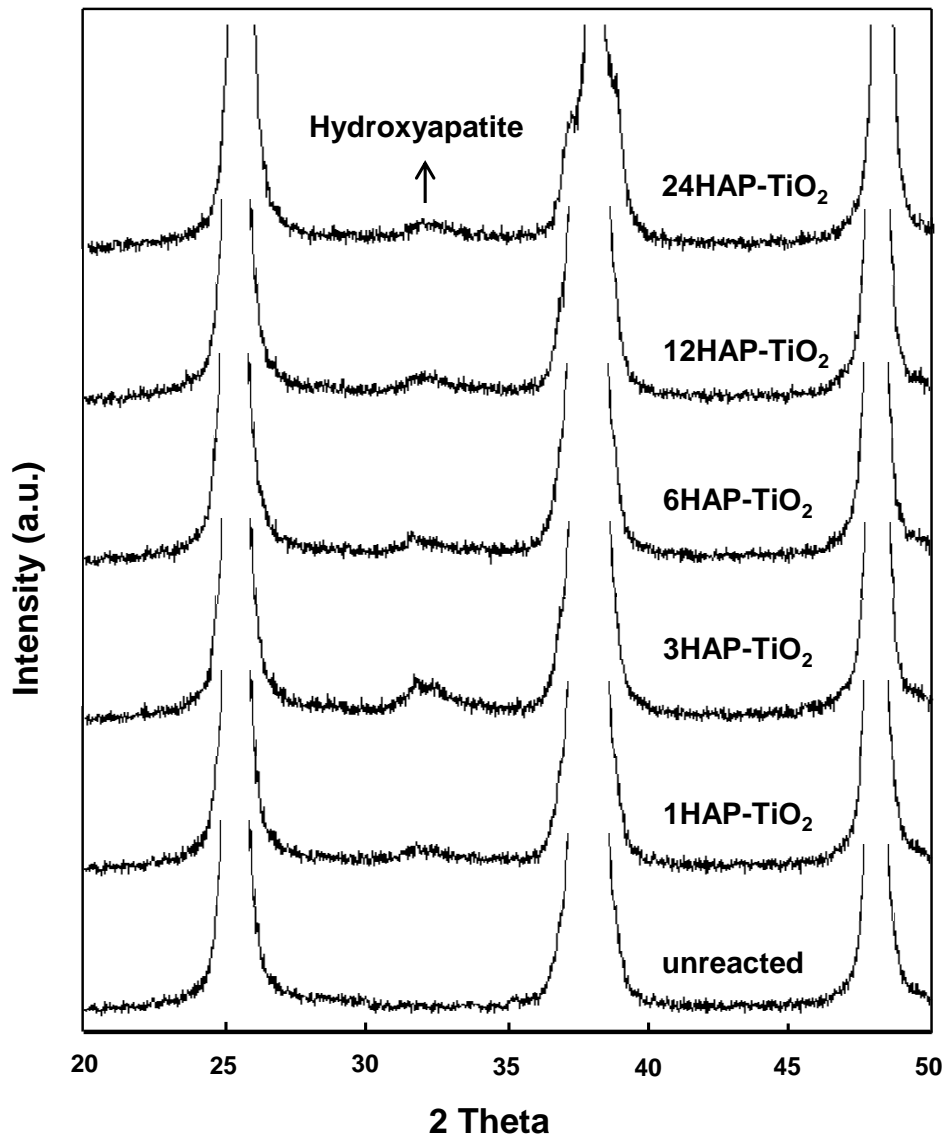


FIGURE 4. 1 XRD patterns of TiO_2 powders before and after immersion in the 10-SBF

The decrease in the intensity of the (101) peak and the appearance of a new peak at 2θ of $\sim 31.6^\circ$ in the diffraction patterns imply the formation of a new phase after immersion of TiO_2 powders in 10 \times SBF. The XRD analyses reveal that the new diffraction peak belongs to the characteristic (211) diffraction plane of hydroxyapatite [HAP, $\text{Ca}_{10}(\text{PO}_4)_6(\text{OH})_2$], JCPDS card # 74-0566. The apatite precipitates on TiO_2 powders possess a small crystallite size or a poorly crystallized structure, judging from the diffraction pattern. Although the HAP, will

be referred to as apatite hereafter, peak could be realized in the patterns of 1HAP-TiO₂, 3HAP-TiO₂, 6HAP-TiO₂, 12HAP-TiO₂, and 24HAP-TiO₂, it is absent in the pattern of unreacted TiO₂. Such results are in good agreement with other researchers [7,71]. The intensity of the HAP peak increased slightly in the TiO₂ powders immersed in 10×SBF up to 3 h but, afterwards it did not seem to change with further immersion durations implying that apatite precipitation on TiO₂ powders is limited in this immersion conditions and does not increase with increasing immersion durations in 10×SBF beyond 3 h. Therefore, the rest of this study was conducted only on unreacted TiO₂, 1HAP-TiO₂, 3HAP-TiO₂, and 6HAP-TiO₂.

Figure 4.2 shows the FTIR spectra of TiO₂ powders before and after immersion in 10×SBF for various durations. An obvious change in the spectrum was observed after immersion of TiO₂ powders in 10-SBF. The intense and broad bands at 3370 and 1640 cm⁻¹ were assigned to the O-H stretching and bending, respectively [7,72]. The intense bands due to PO₄³⁻ group at 400-600 and 1000-1100 cm⁻¹ were observed in the apatite precipitated TiO₂ powders [17]. Absorption peaks at 1421 and 1460 cm⁻¹ attributed to the carbonate ions [70,72] have not been observed. Therefore samples are only composed of HAP. Small bands shown between wavelengths of 2300 and 1800 cm⁻¹ belongs to attenuated total reflectance (ATR) accessory crystal therefore does not transmit from the samples.

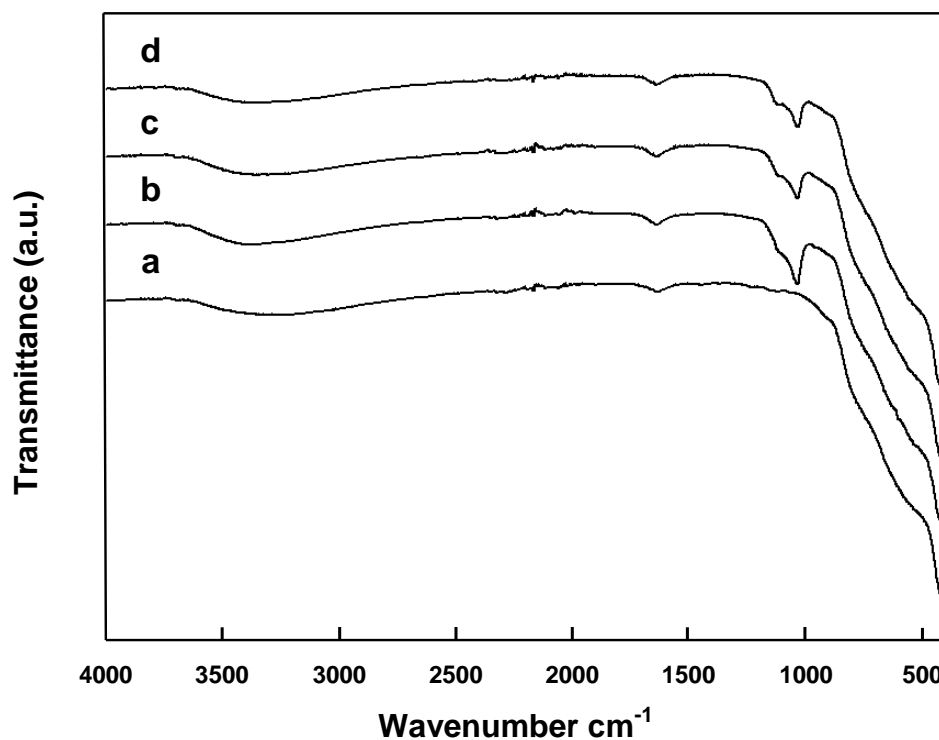
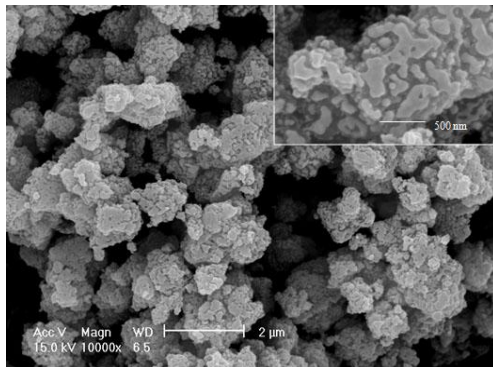


FIGURE 4. 2 FTIR spectra of a) unreacted TiO_2 b) 1HAP- TiO_2 , c) 3HAP- TiO_2 and d) 6HAP- TiO_2 powders

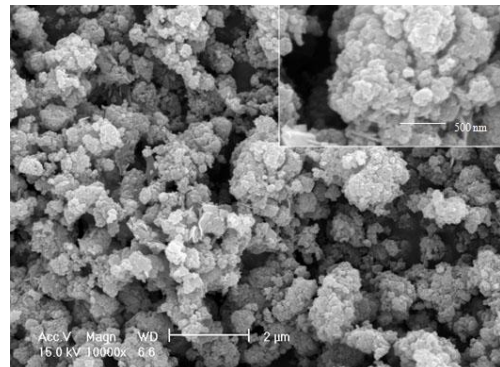
4.2.2. Scanning Electron Microscope (SEM) and Energy Dispersive Spectroscopy (EDS)

The surface morphologies of TiO_2 powders before and after immersion in 10-SBF solution for different durations are indicated in Figure 4.3. It is clear that surface morphology of TiO_2 powders changes after immersion in 10-SBF. The surface of unreacted TiO_2 is clean and smooth as seen in Figure 4.3(a). The surfaces of 1HAP- TiO_2 and 3HAP- TiO_2 are, on the other hand, rough and coarse as shown in Figures 4.3(b) and 4.3(c), respectively. Surface irregularities increased as immersion time increased signifying that more apatite crystals, as suggested by the XRD results, were deposited on the surface. When immersion duration was increased to 6 h, the surface morphology resembled the morphology of 1HAP- TiO_2 as seen in Figure 4.3(d). The alteration in surface

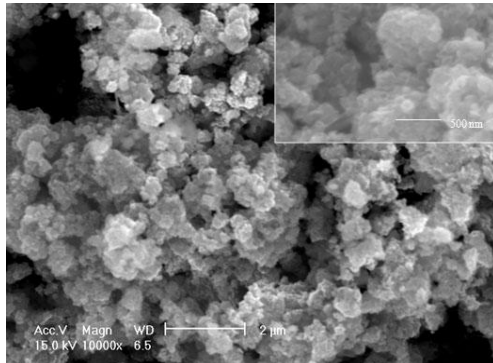
morphology with increasing immersion duration beyond 3 h is attributed to a decrease in the Ca and P ion concentrations in 10-SBF with time which induces Ca and P ions to be re-dissolved. Therefore, some amounts of Ca and P ions detach from TiO_2 surface and re-dissolve in 10-SBF. Apatite formation does not continue anymore. Not much difference is observed in the apatite deposition on the surfaces of 3HAP- TiO_2 and 6HAP- TiO_2 . SEM analyses are consistent with the results obtained in the XRD analyses.



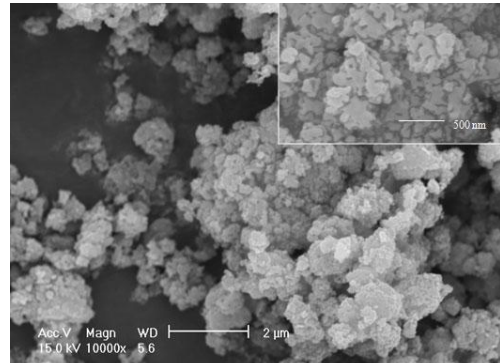
a) unreacted



b) 1HAP- TiO_2



c) 3HAP- TiO_2



d) 6 HAP- TiO_2

FIGURE 4. 3 SEM micrographs of a) unreacted TiO_2 , b) 1HAP- TiO_2 , c) 3HAP- TiO_2 and d) 6HAP- TiO_2

The EDS analyses of TiO₂ powders immersed in 10-SBF for 1, 3, and 6 h proved that Ca and P present in the samples. Amount of apatite precipitates on TiO₂ powders immersed in 10-SBF for 1, 3, and 6 h are given in Table 4.1. The EDS spectra of 1HAP-TiO₂, 3HAP-TiO₂ and 6HAP-TiO₂ are shown in Figure 4.4.

TABLE 4. 1 Weight percentage of hydroxyapatite on TiO₂ powders

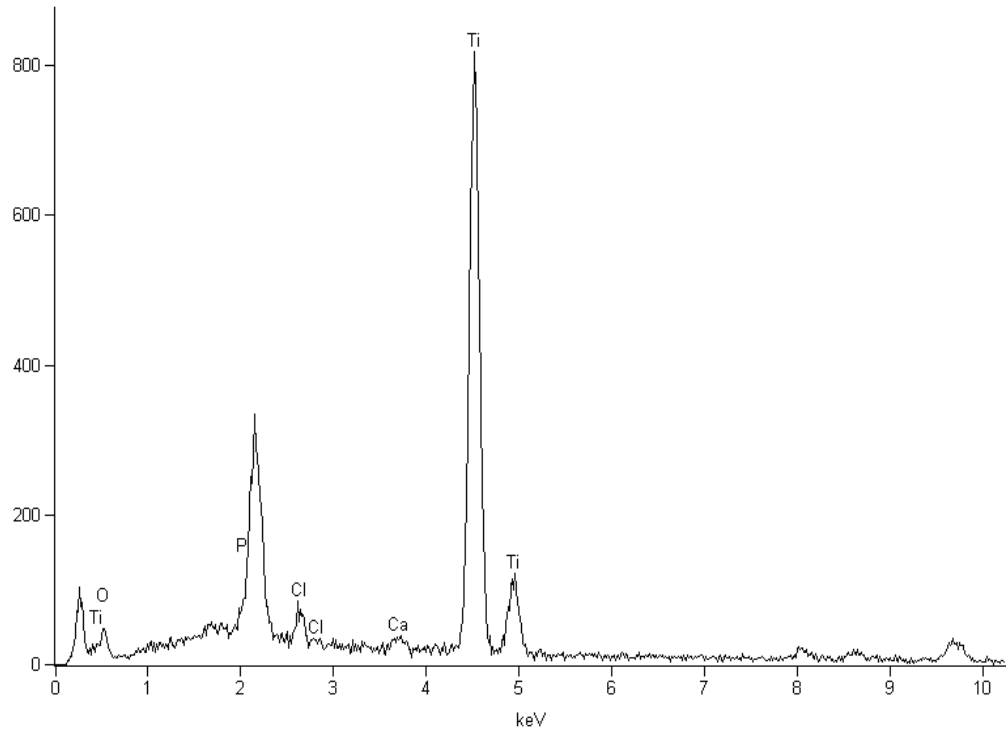
Powder	Hydroxyapatite (wt %)
Unreacted	0
1HAP-TiO ₂	8.77
3HAP-TiO ₂	10.52
6HAP-TiO ₂	10.35

The weight percent concentrations of CaO and P₂O₅ in the powders immersed in 10-SBF for 1, 3, and 6 h are given in Table 4.2. 3HAP-TiO₂ with Ca/P ratio of 1.63, slightly less than that of the adult human bone, offers the most satisfactory results in terms of Ca/P ratio of the apatite formation on the surface of TiO₂ powders. The reason why Ca/P atomic ratio of 1.67 is not achieved is related to two aspects: on the one hand, the SBF solution employed throughout this thesis study is not completely consistent with human blood plasma; on the other hand, the condition in our experiments could not completely follow that in human body.

TABLE 4. 2 Weight concentrations of CaO and P₂O₅ in TiO₂ powders after immersion in SBF

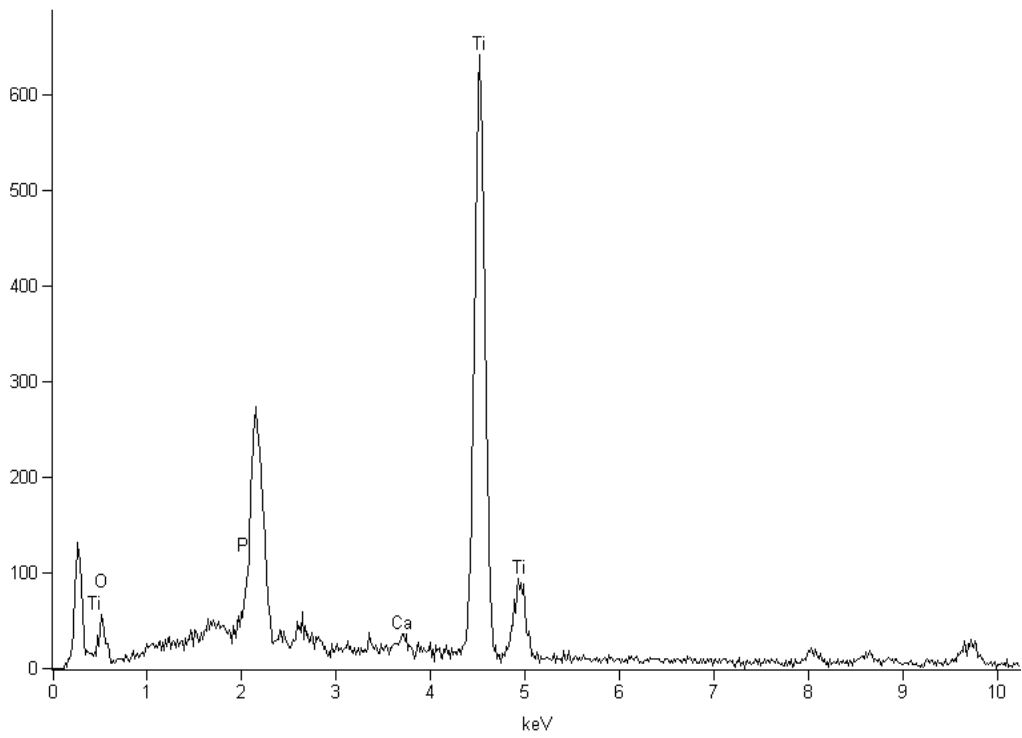
Oxides	Weight Concentration After Immersion in SBF for		
	1 h	3 h	6 h
CaO	4.82	5.81	5.27
P₂O₅	3.79	4.52	4.91
Ca/P	1.59	1.63	1.36

Full scale counts: 817



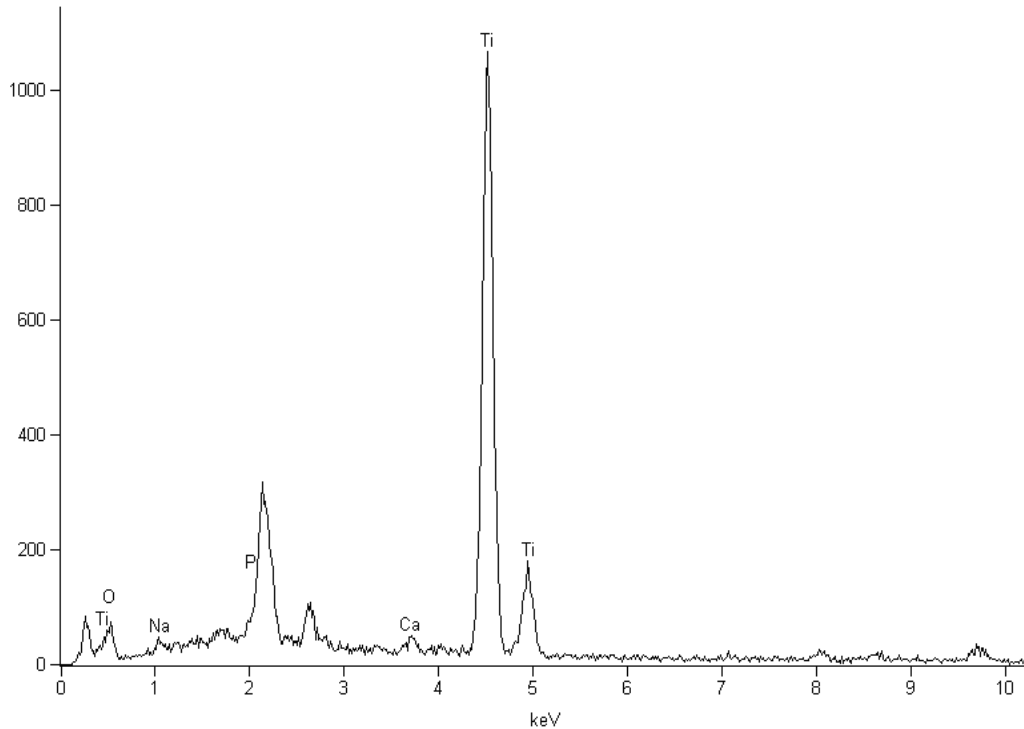
a) 1HAP-TiO₂

Full scale counts: 641



b) 3HAP-TiO₂

Full scale counts: 1066



c) 6HAP-TiO₂

FIGURE 4. 4 EDS analysis results for a) 1HAP-TiO₂, b) 3HAP-TiO₂, and c) 6HAP-TiO₂

The EDS spectra of the apatite deposited TiO₂ powders show Ti peaks signifying that the apatite deposition is non-continuous and may allow light to penetrate into TiO₂ powder. Shi et al. [72] studied biomimetic apatite layer formation on plasma-sprayed titanium coatings and reported that the Ti peaks in the EDS spectrum indicate a thin, non-continuous layer of Ca-P layer. However, when there are no Ti peaks, whole surface of the Ti should be covered with Ca-P layer where the thickness of the Ca-P layer formed exceeds several micrometers.

Consistent with the results taken from the X-Ray and SEM analyses, the EDS analysis suggested that TiO₂ powders could induce the nucleation and growth of apatite and the apatite precipitates could be obtained on TiO₂ powders. The heterogeneous nucleation and growth of apatite can only or mainly form on a negatively charged interface. A negatively charged surface with functional groups might be effective for the apatite formation on a substrate [73]. As confirmed by EDS analyses, after TiO₂ powders were immersed in 10-SBF for 3

h, the amount of deposited apatite increased noticeably. Such results are in good agreement with other researchers [7,71,74].

The pH of the solution has a profound effect on the apatite nucleation. When pH of the solution is greater than 6.0, the apatite nucleation is easily formed due to the negatively charged TiO₂ surface [7]. Within the range of 7.25-7.40 pH value, negatively charged Ti-OH groups are formed on the surface of TiO₂ powders in the SBF solution [59]. When TiO₂ powders are immersed in 10-SBF, the apatite nuclei are formed on TiO₂ powders due to the electrostatic interaction between negatively charged TiO₂ surface and the ions in SBF. It has been reported that the electrostatic interaction is the main factor in inducing Ca-P nucleation [74]. After the nucleation, the TiO₂ surface does not act as the center of nucleation, and the apatite formed on TiO₂ powder becomes the center of nucleation and growth. The calcium ions, phosphate ions and other minor ions (i.e. CO₃²⁻ and Mg²⁺) in SBF deposit spontaneously on the TiO₂ surface to form apatite precipitates because the SBF solution was supersaturated with respect to apatite.

The apatite deposition can not take place without calcium ions since the Ti-OH groups first combine with some amount of Ca²⁺ ions in SBF to form a kind of calcium titanate. The formed calcium titanate then combines with PO₄³⁻ ions. Subsequently, large amounts of Ca²⁺ and PO₄³⁻ ions are adsorbed onto the surface of the TiO₂ powders to form apatite [51]. Schematic illustration for the possible mechanism of apatite precipitation on TiO₂ powder in SBF is shown in Figure 4.5.

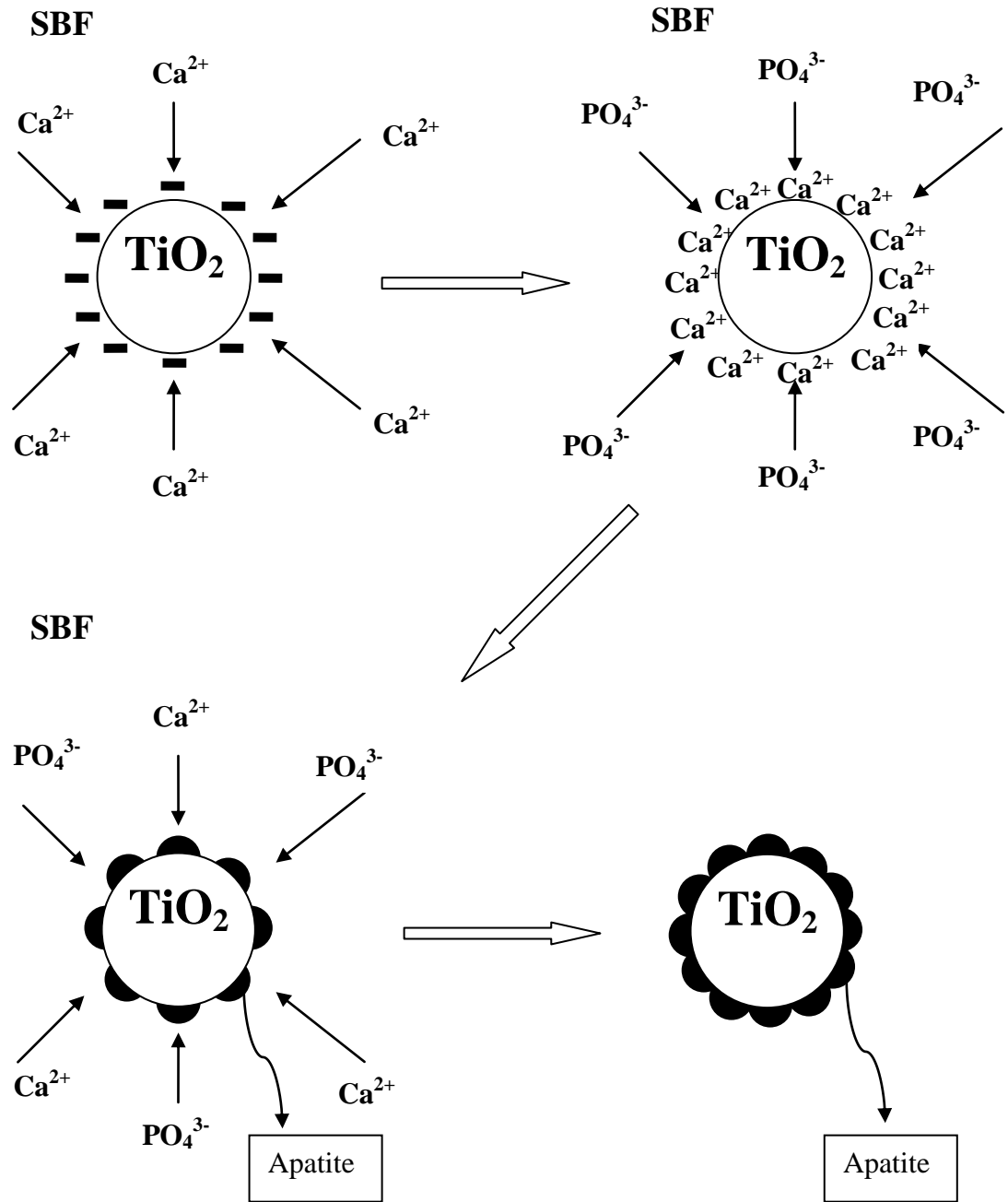


FIGURE 4. 5 Schematic diagram showing the possible mechanism of apatite formation on TiO_2 powder in 10-SBF

Yang et.al. [7] observed no obvious change in the phosphate ion concentration throughout the immersion duration, whereas the calcium ion concentration first decreased abruptly and then became stable. For this reason amount of apatite increases on TiO_2 surface when the powders are immersed in 10-SBF up to 3 h,

but tends to decrease when the immersion time is increased as explained earlier.

Consistent with the results taken from the X-Ray and SEM analyses, the EDS analysis suggested that 3 h immersion in SBF offers the best result in terms of the apatite formation on the surface of TiO₂ powders. This is why in the forthcoming part most of the experiments were conducted by using 3HAP-TiO₂ and the attention is focused particularly on these powders

4.3. THE PHOTOCATALYTIC ACTIVITY

4.3.1. Photocatalytic Activity of the Compacts of PMMA and TiO₂ Powders

Photocatalytic activity of the compacts composed of PMMA and TiO₂ powder were examined according to the procedure described in Section 3.6.1. The variation of weight in compacts formed by mixing PMMA and the TiO₂ powders immersed in 10-SBF for 1, 3, and 6 h with UV exposure time is shown in Figure 4.6. All samples exhibited weight loss during the first 30 min. At the end of 360 min, the samples of 1HAP-TiO₂ and 3HAP-TiO₂ indicated 0.13% weight loss, whereas 6HAP-TiO₂ sample indicated 0.11% weight loss. Not much difference was detected among these three samples. However, the unreacted TiO₂ sample showed more weight loss (0.24%) compared to the apatite deposited samples.

From the results presented in Figure 4.6, the following points should be highlighted. First of all, all of the powders did exhibit photocatalytic properties. PMMA is used as supporting material on the photocatalytic TiO₂ [11,66,75]. However, photocatalytic TiO₂ degrades the coated PMMA. Findings in the experiments revealed that via apatite deposition on the surface of TiO₂ powders, the degradation of PMMA could be hindered. Nonami et al. [11] report that

apatite deposition blocks the contact between TiO_2 powders and PMMA. As a result, unreacted TiO_2 shows the fastest weight loss with respect to UV exposure time, whereas the apatite-deposited TiO_2 powders degraded at a much slower rate.

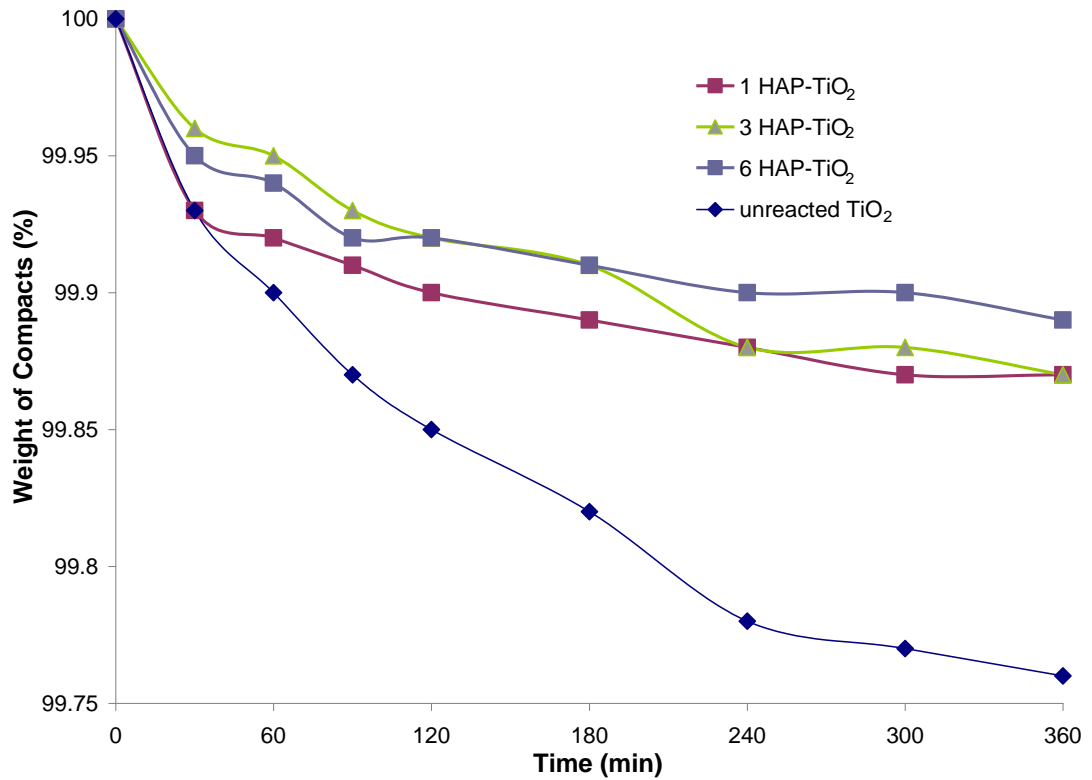


FIGURE 4. 6 Percent weight change in the compacts of PMMA and TiO_2 powders with UV exposure time

The decrease in the weight of compacts with UV exposure time is shown separately in Figure 4.7. It can be seen that, the apatite deposited powders lose nearly 0.01 g in weight, and the unreacted TiO_2 loses 0.02 g in weight. Amount of PMMA decomposition decreased when apatite is deposited on TiO_2 powders.

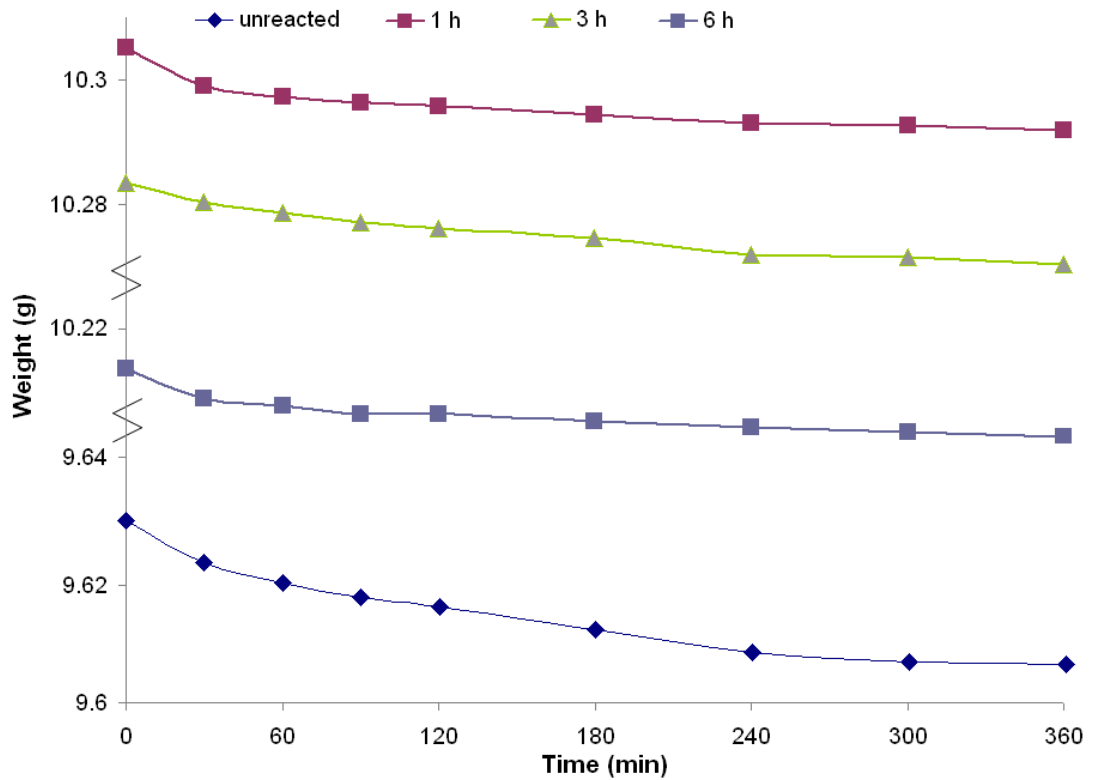


FIGURE 4. 7 Weight change in the compacts of PMMA and TiO₂ powders with UV exposure time

4.3.2. Photocatalytic Activity of TiO₂ Powders in Methylene Blue (MB) Solution

A variety of experiments was conducted to measure the photocatalytic activity of TiO₂ powders in MB solution according to the procedure as described in Section 3.6.1. The variations in light absorption and MB concentration with respect to UV exposure time for unreacted TiO₂ and apatite deposited TiO₂ powders are shown in Figures 4.8 and 4.9, respectively.

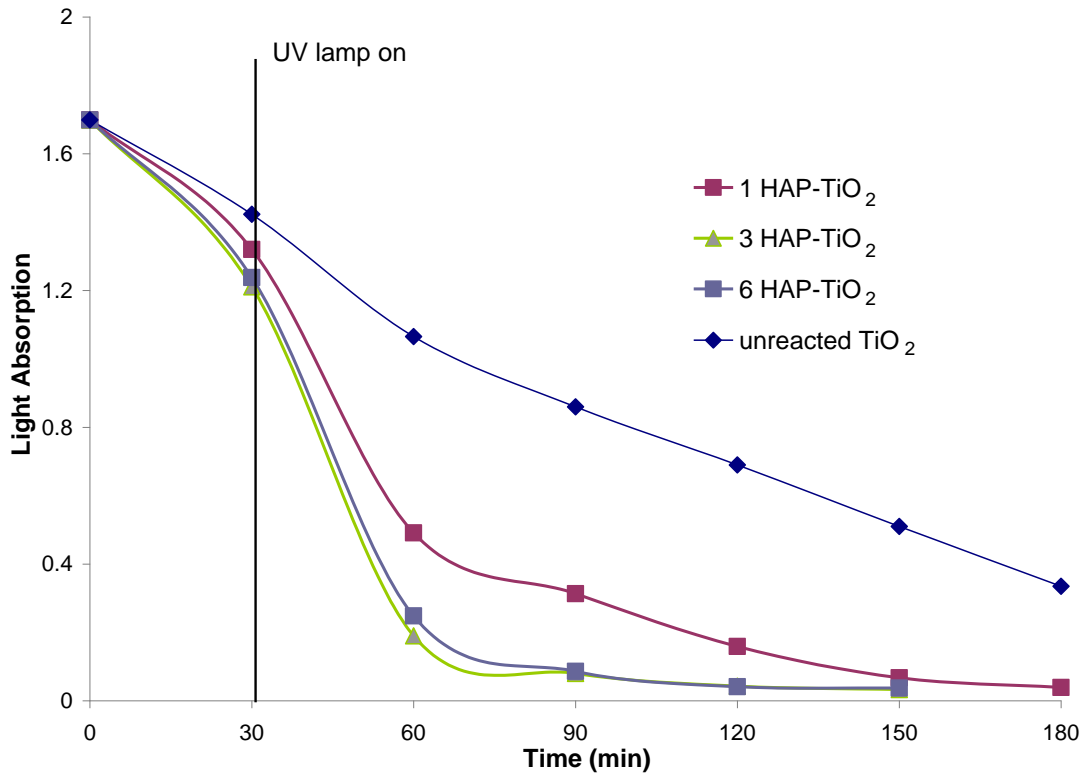


FIGURE 4. 8 Variation in light absorption with UV exposure time for unreacted TiO_2 and apatite deposited TiO_2 powders

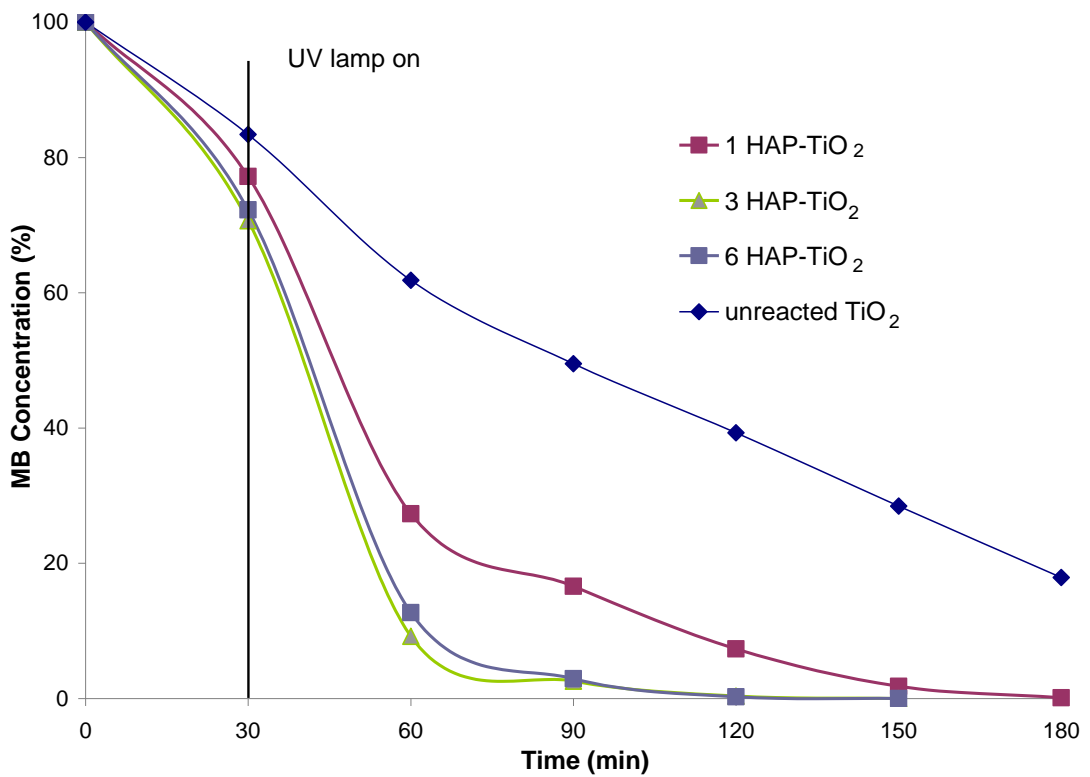


FIGURE 4. 9 Variation of percent MB concentration with UV exposure time for unreacted TiO_2 and apatite deposited TiO_2 powders

It is clear that all powders can photocatalytically decompose MB. Absorption of MB increases when UV exposure time is increased. At a given UV exposure time, the apatite deposited TiO₂ powders show better photocatalytic activity than unreacted TiO₂. The initial light absorption value of the MB solution was 1.699 for all TiO₂ powders. After 30 min in dark, the light absorption values of the MB solution for unreacted TiO₂, 1HAP-TiO₂, 3HAP-TiO₂ and 6HAP-TiO₂ were 1.423, 1.320, 1.211, and 1.238, respectively. After the light was turned on, during the second 30 min period, the light absorption values of the MB solution for the apatite deposited powders decreased. When the UV exposure duration exceeds 30 min, the rate of decrease in the light absorption slows down, probably due to the decrease in the concentration of the MB solution. The complete decomposition time (the time necessary for reaching the light absorption value of de-ionized water) of MB for unreacted TiO₂ was 4 h and decreased to 2.5 h for 1HAP-TiO₂, and to 2 h for 3HAP-TiO₂. The complete decomposition time of MB for 6HAP-TiO₂ was more or less the same as that for 3HAP-TiO₂. Findings are in accord with those reported in the literature for the apatite-coated TiO₂ substrates [44,76].

Only 16.61% of MB was absorbed by unreacted TiO₂ before UV light was turned on (when the powders were kept in dark). Absorption of MB increased under the same experimental conditions when apatite was deposited on TiO₂ powders. The percentage of MB absorbed by 1HAP-TiO₂, 3HAP-TiO₂ and 6HAP-TiO₂ in dark were 22.81%, 29.36% and 27.74%, respectively. It has been recognized that photocatalytic activity of TiO₂ powders was improved when apatite was deposited on the surface and when the immersion duration in 10-SBF was increased up to 3 h. Beyond that, photocatalytic activity of TiO₂ powders did not seem to change with increasing immersion time in 10-SBF. The light absorption values and MB concentration in 3HAP-TiO₂ and 6HAP-TiO₂ were almost the same for a given UV exposure time.

Figure 4.10 shows the plot of $\ln([MB]_0/[MB])$ vs. UV exposure time for the unreacted and apatite deposited TiO₂ powders. The correlation coefficients (R^2) of the powders are also indicated in Figure 4.10. The slope of the curves in the figure gives the values for K_{ap} . The values of K_{ap} and R^2 for all powders are listed

in Table 4.3. The correlation coefficient here represents a measure of how well the predicted values from the Langmuir-Hinshelwood kinetic model fit with the data obtained. The strength of the relationship between the predicted values and actual values increases with the correlation coefficient. A perfect fit gives a coefficient of 1.0. Therefore, the higher the correlation coefficient, the better the fit with the model is.

3HAP-TiO₂ offers the best result in terms of the K_{ap} value which implies that 3HAP-TiO₂ has the best photocatalytic activity among the other powders. Results reveal that the higher the apatite deposition the better the photocatalytic activity. The R² values in this experiment are close to a coefficient of 1.0. As reported also by Park [77], the decomposition of MB fits the Langmuir–Hinshelwood kinetic model.

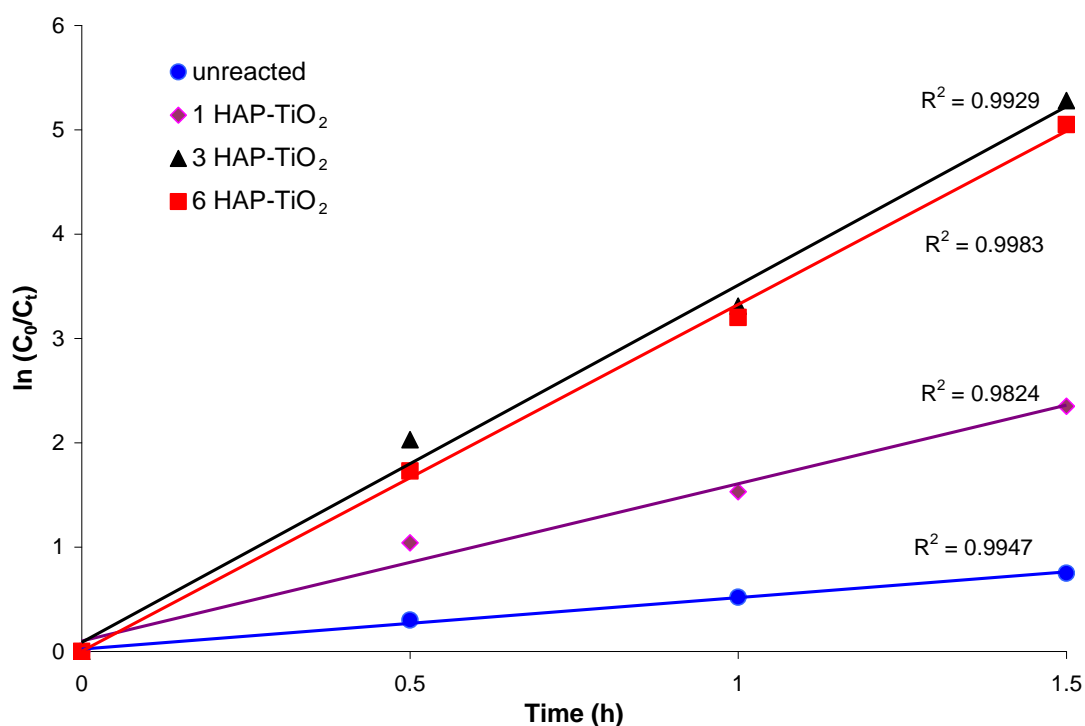


FIGURE 4. 10 Variation of $\ln([MB]_0/[MB])$ with UV exposure time for the unreacted and apatite deposited TiO₂ powders

TABLE 4. 3 Values for the reaction rate constant and correlation coefficient for the photocatalytic decomposition of MB

	Unreacted TiO ₂	1HAP-TiO ₂	3HAP-TiO ₂	6HAP-TiO ₂
$K_{ap}(h^{-1})$	0.51	1.52	3.48	3.39
R^2	0.9947	0.9824	0.9929	0.9983

In the second set of experiments involving different MB concentrations in solution, the MB concentrations were adjusted to 2.5, 5, and 10 mg/l. MB decomposition was measured only on unreacted TiO₂ powders. The results were presented in Figures 4.11 and 4.12.

Light absorption values of all samples decreased with increasing UV exposure time. Light absorption value for the sample with the lowest MB concentration (2.5 mg/l) decreased from 0.625 to 0.037 in 150 min, whereas for the sample with the moderate MB concentration (5 mg/l) it decreased from 1.209 to 0.037 in 180 min. Light absorption value for the sample with the highest MB concentration (10 mg/l), on the other hand, decreased from 1.699 to 0.335 in 180 min. The lower the MB concentration in the solution, the faster MB decomposes photocatalytically [76]. Figure 4.12 indicates the decrease in MB percentage with UV exposure time. When the samples were in dark, 2.5, 5, and 10 mg/l MB concentrations decreased by 37.68%, 17.92% and 16.61%, respectively.

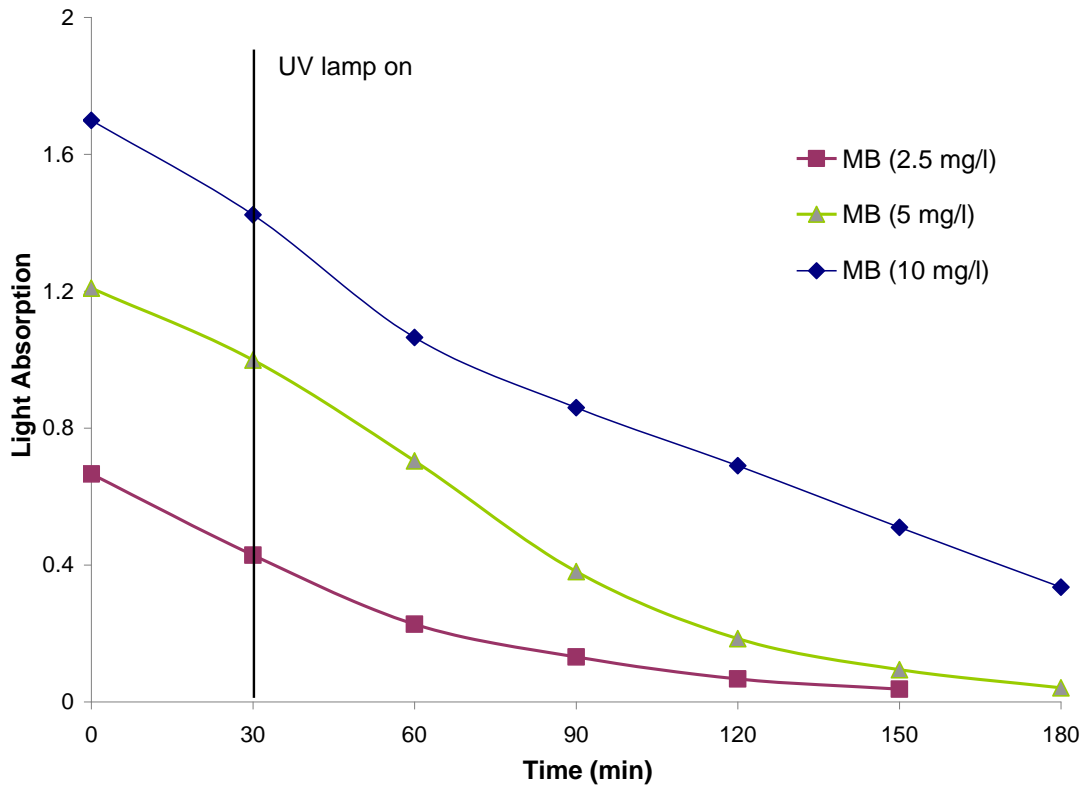


FIGURE 4. 11 Variation in light absorption with UV exposure time for different MB concentrations in the solution

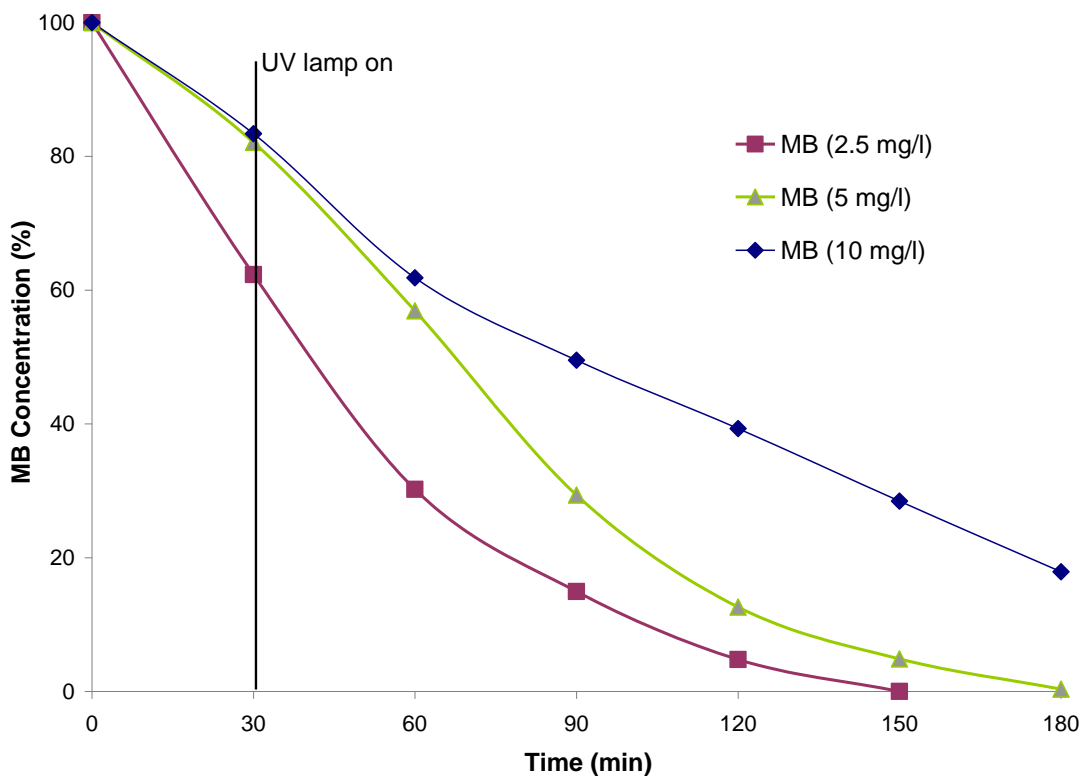


FIGURE 4. 12 Variation of percent MB concentration with UV exposure time for different MB concentrations in the solution

Figure 4.13 illustrates the plot of $\ln([MB]_0/[MB])$ vs. UV exposure time for different MB concentrations, and corresponding correlation coefficients. The reaction rate parameters for varying MB concentrations are presented in Table 4.4.

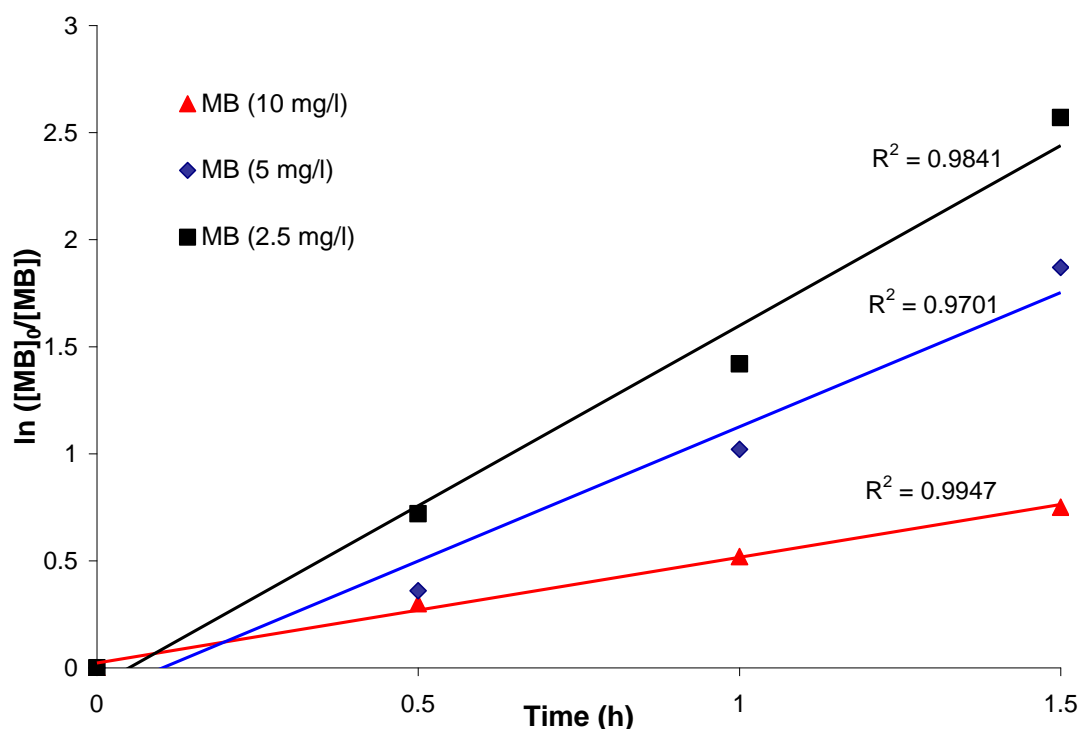


FIGURE 4. 13 Variation of $\ln([MB]_0/[MB])$ with UV exposure time for different MB concentrations in the solution

TABLE 4. 4 The reaction rate constant and correlation coefficient for unreacted TiO_2 for different MB concentrations in the solution

	MB (2.5 mg/l)	MB (5 mg/l)	MB (10 g/l)
$K_{ap} (h^{-1})$	1.63	1.17	0.51
R^2	0.9841	0.9701	0.9947

As the MB concentration in the solution increases, the MB decomposition rate decreases. The MB decomposition rate for 2.5, 5, and 10 mg/l MB concentrations was 1.63, 1.17, and 0.51, respectively. The results obtained here is also consistent with those reported by Shimizu et al. who stated that the degradation ratio is inversely proportional to the initial MB concentration [78]. Also, the reaction rate computed for 5 mg/l MB solution is similar to that reported

by Syoufian and Nakashima [18]. Since R^2 values are close to 1.0 in this case, it could be said that the decomposition of MB fits the Langmuir–Hinshelwood kinetic model.

In the third set of experiments, instead of unreacted TiO_2 , 3HAP- TiO_2 was used since 3HAP- TiO_2 offered better results in terms of apatite formation and photocatalytic activity. The findings obtained from the third set of experiments are shown in Figures 4.14 and 4.15. As the MB solution concentration for the 3HAP- TiO_2 samples increases, the MB decomposition rate decreases. A comparison of Figures 4.11 and 4.12 with Figures 4.14 and 4.15 reveals that the results of 3HAP- TiO_2 are similar to those given for unreacted TiO_2 . However, photocatalytic decomposition experiments of 3HAP- TiO_2 resulted in a considerable shorter time. That is; the samples containing lower MB concentrations decomposed in only 90 min. When UV lamp was off during the first 30 min, the MB absorption was nearly 55% for the samples containing 5 and 2.5 mg/l MB; whereas it was nearly 30% for the sample containing 10 mg/l MB.

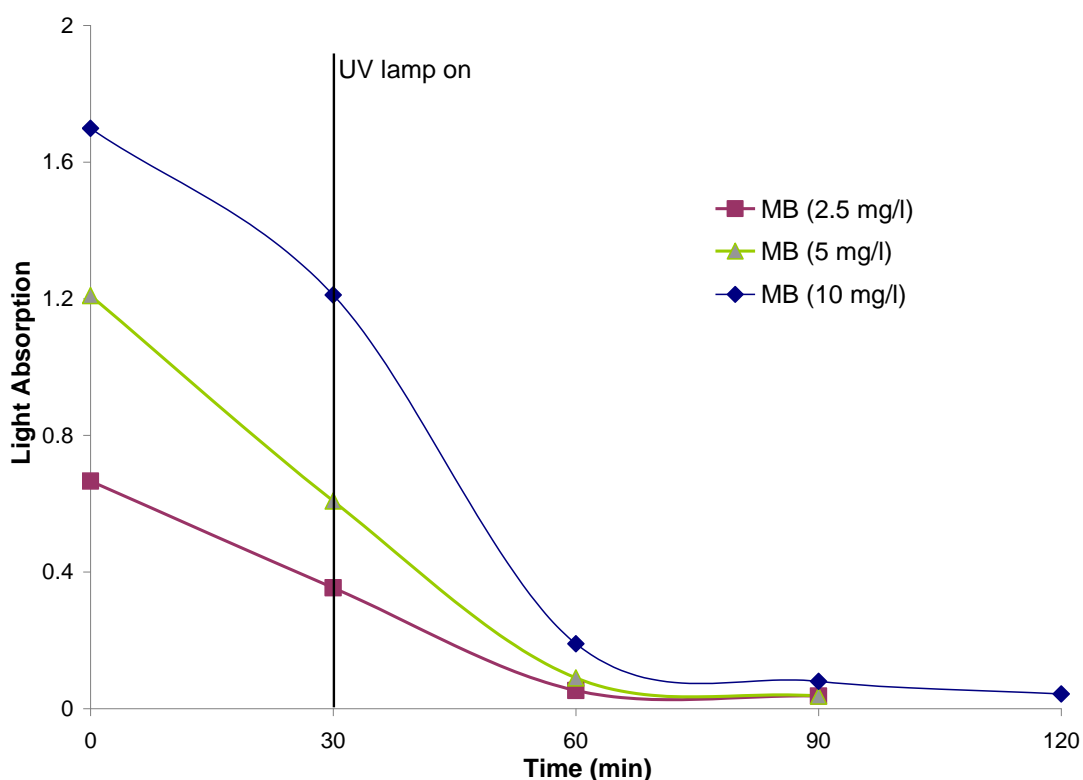


FIGURE 4. 14 Variation in light absorption with UV exposure time for different MB concentrations in the solution

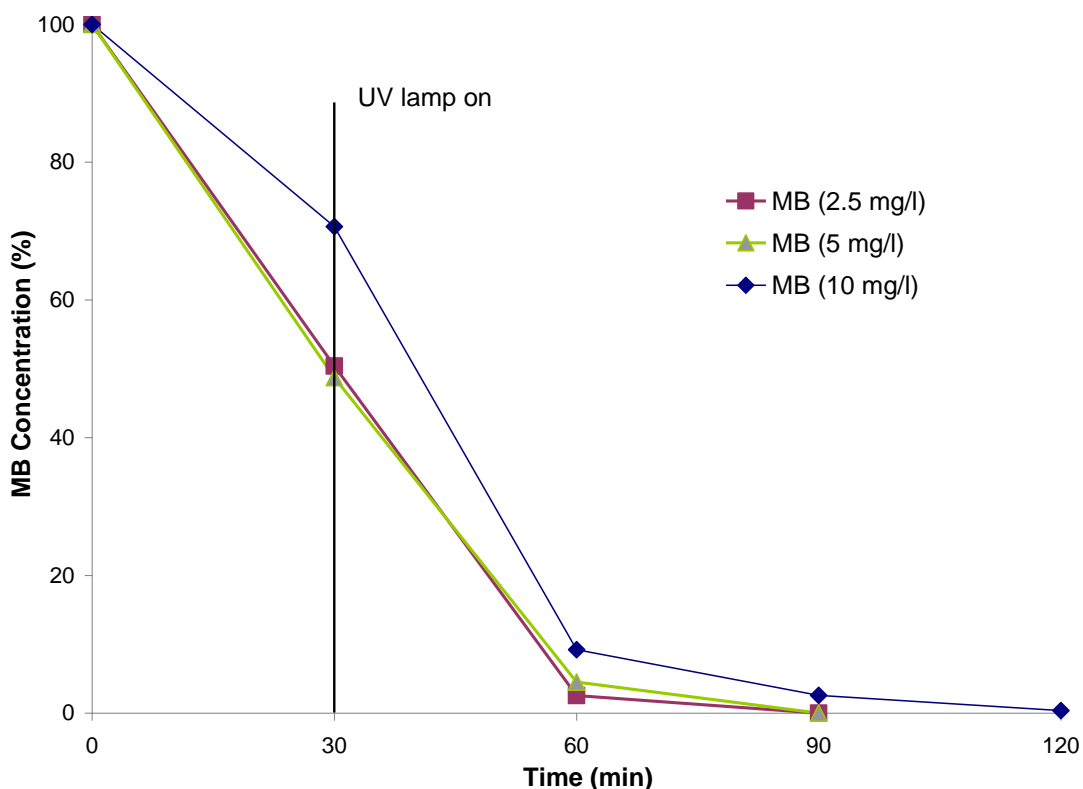


FIGURE 4. 15 Variation of percent MB concentration with UV exposure time for different MB concentrations in the solution

The plot of $\ln([MB]_0/[MB])$ vs. UV exposure time for different MB concentrations and their correlation coefficients were not drawn since only one data was available. Table 4.5 presents the reaction rates for 3HAP-TiO₂ in varying MB concentrations. The MB decomposition rate for 2.5, 5, and 10 mg/l MB concentrations was 5.96, 5.12, and 4.06, respectively.

TABLE 4. 5 The reaction rate constant for 3HAP-TiO₂ of different MB concentrations in solution

	MB (2.5 mg/l)	MB (5 mg/l)	MB (10 mg/l)
$K_{ap} (h^{-1})$	5.96	5.12	4.06

In the fourth set of experiments, the amount of the unreacted TiO₂ was changed while the concentration of MB solution was kept constant at 10 mg/l. The results obtained from the fourth set of experiments are shown in Figures 4.16 and 4.17.

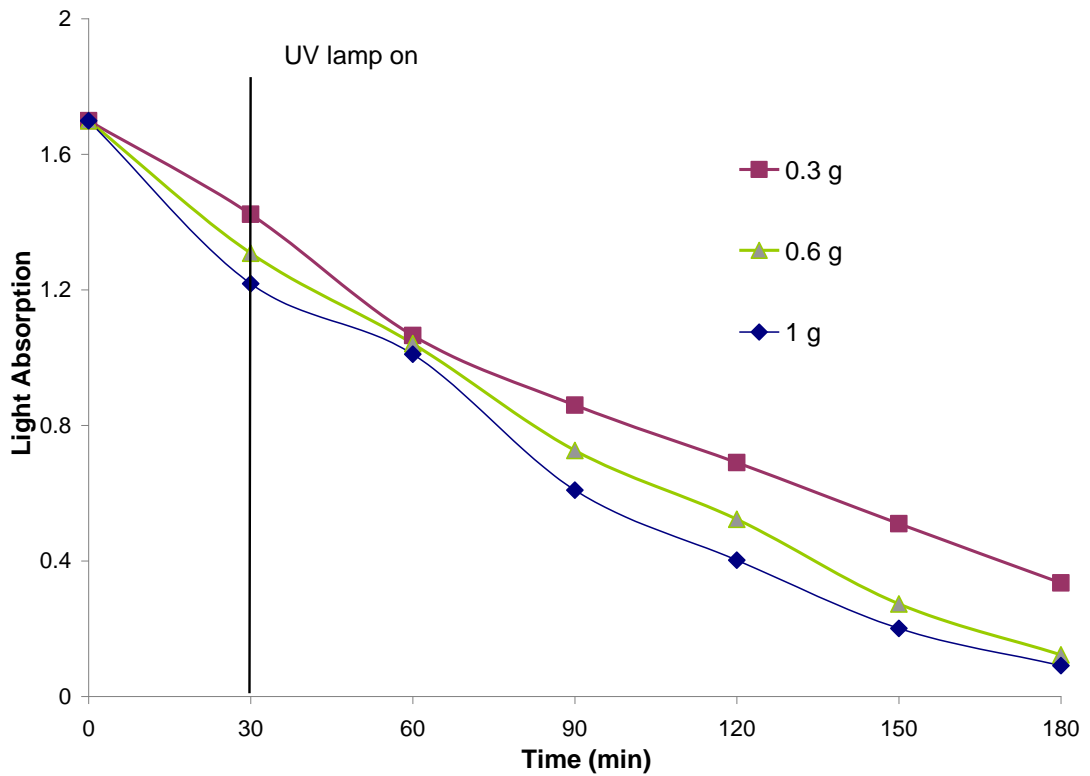


FIGURE 4. 16 Variation in light absorption with UV exposure time for different amounts of unreacted TiO₂ in the solution

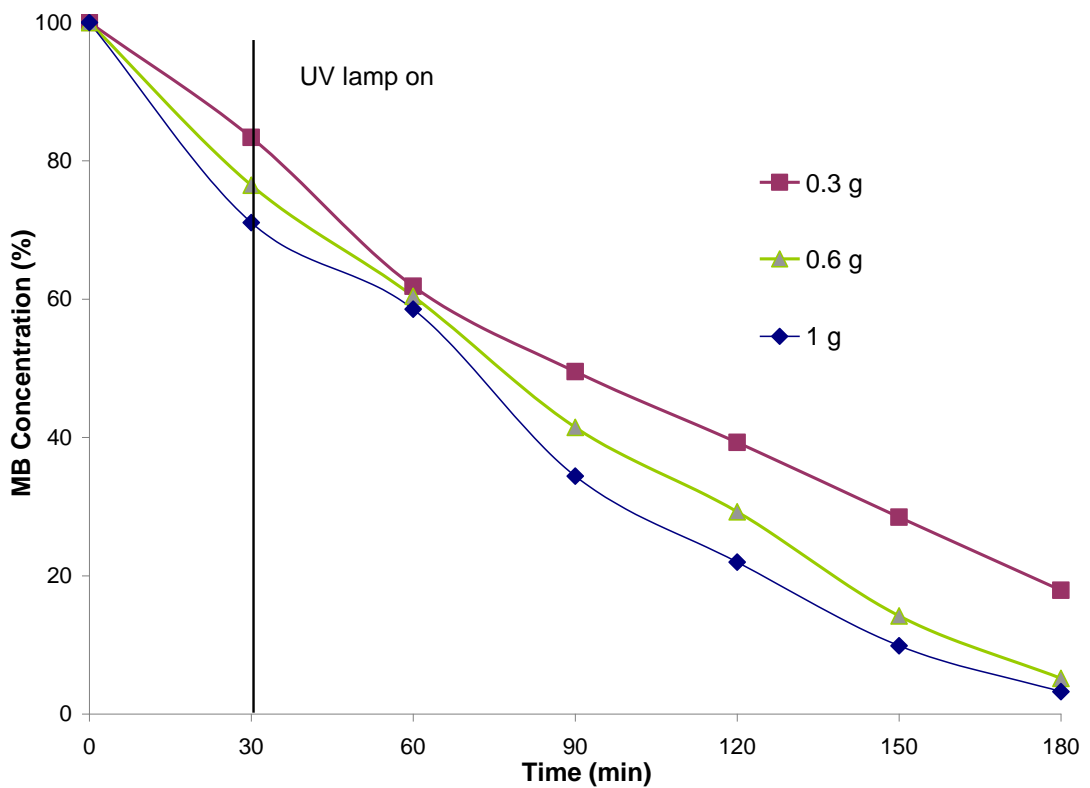


FIGURE 4. 17 Variation of percent MB concentration with UV exposure time for different amounts of unreacted TiO₂ in the solution

The results reveal that the decomposition of MB becomes faster as the amount of TiO₂ is increased. In dark, the concentrations of MB decreased by 16.61% for 0.3 g TiO₂, 23.53% for 0.6 g TiO₂, and 28.95% for 1.0 g TiO₂. After 180 min, the light absorption value for 1 g of unreacted TiO₂ was 0.091. It was 0.123 for 0.6 g, and was 0.335 for 0.3 g.

The plot of $\ln([MB]_0/[MB])$ vs. UV exposure time for different amounts of TiO₂ in the solution and their correlation coefficients are shown in Figure 4.18. Table 4.6 presents the reaction rates for different amounts of TiO₂ in the solution.

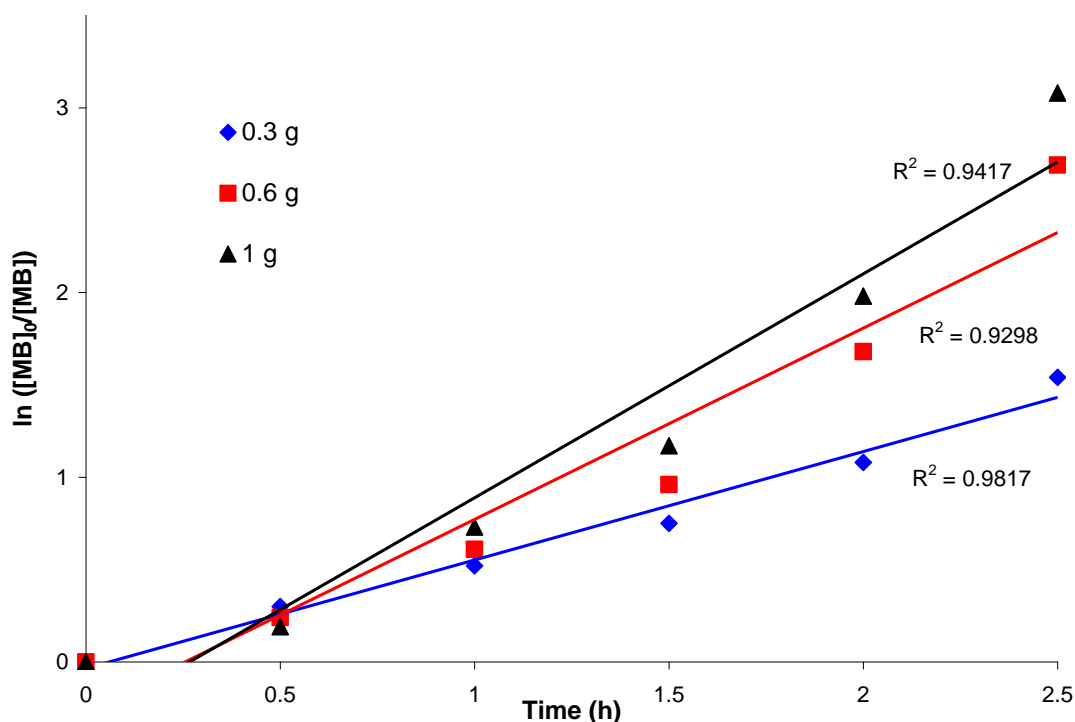


FIGURE 4. 18 Variation of $\ln([MB]_0/[MB])$ with UV exposure time for different amounts of unreacted TiO₂ in the solution

TABLE 4. 6 The reaction rate constant and correlation coefficient for different amounts of unreacted TiO₂ in the solution

	0.3 g TiO ₂	0.6 g TiO ₂	1 g TiO ₂
$K_{ap} (h^{-1})$	0.57	0.93	1.08
R^2	0.9817	0.9298	0.9417

As the amount of TiO_2 in the solution increases, the reaction rate also increases. In this particular case, the reaction rate for 0.3 g TiO_2 was 0.57 and increased to 0.93 for 0.6 g TiO_2 and to 1.08 for 1 g TiO_2 . The R^2 values for 1 g, 0.6 g, and 0.3 g TiO_2 were 0.9817, 0.9298, and 0.9417, respectively. These values were relatively lower than the ideal 1.0. This might indicate that the decomposition of MB solution deviates relatively from the Langmuir–Hinshelwood kinetic model. The degradation efficiency improves with increasing TiO_2 concentration due to the increase in total surface area available for contaminant adsorption.

In the fifth set of experiments, again the MB concentration in the solution was kept constant at 10 mg/l but, instead of unreacted TiO_2 different amounts of 3HAP- TiO_2 was used for comparison between these powders. The results obtained from the fifth set of experiments are shown in Figures 4.19 and 4.20.

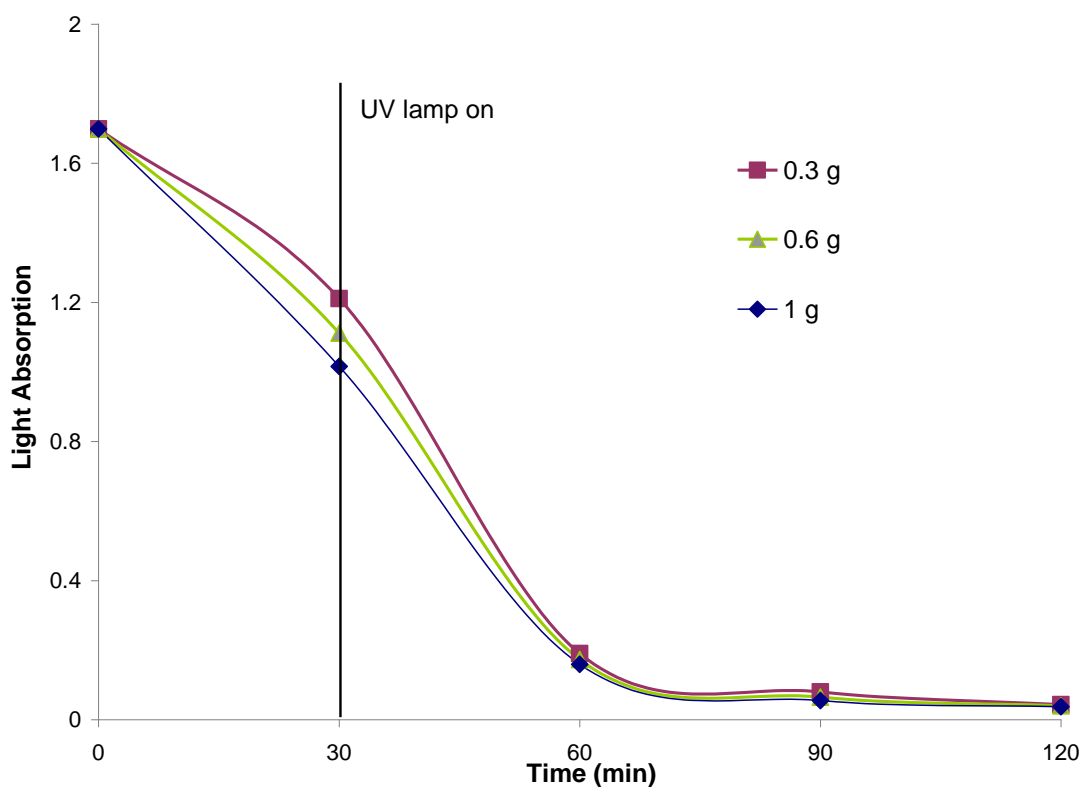


FIGURE 4. 19 Variation in light absorption with UV exposure time for different amounts of 3HAP- TiO_2 in the solution

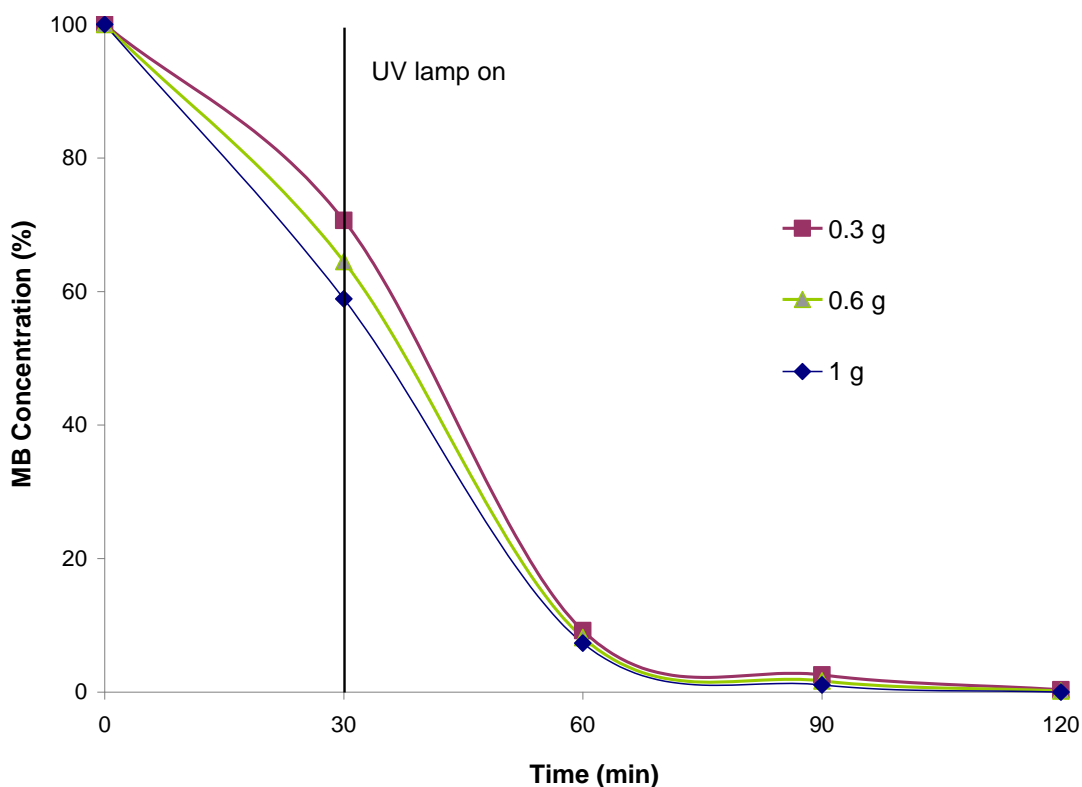


FIGURE 4. 20 Variation of percent MB concentration with UV exposure time for different amounts of 3HAP-TiO₂ in the solution

When a comparison is made between Figures 4.16 and 4.17 and Figures 4.19 and 4.20, 3HAP-TiO₂ offers better results than unreacted TiO₂ in terms of the decomposition of MB from the solution. The absorption of MB increases also as the amount of 3HAP-TiO₂ increases. In dark, 0.3 g 3HAP-TiO₂ absorbs 29.36% of the MB but the absorption increases to 35.52% for 0.6 g, and to 41.10% for 1.0 g. After almost 90 min., all samples completely decomposed. It is obvious that increasing additions of TiO₂ results in faster decomposition of MB.

The plot of $\ln([MB]_0/[MB])$ vs. UV exposure time for different amounts of 3HAP-TiO₂ in the solution and their correlation coefficients are shown in Figure 4.21. Table 4.7 presents the reaction rates for different amounts of 3HAP-TiO₂ in the solution.

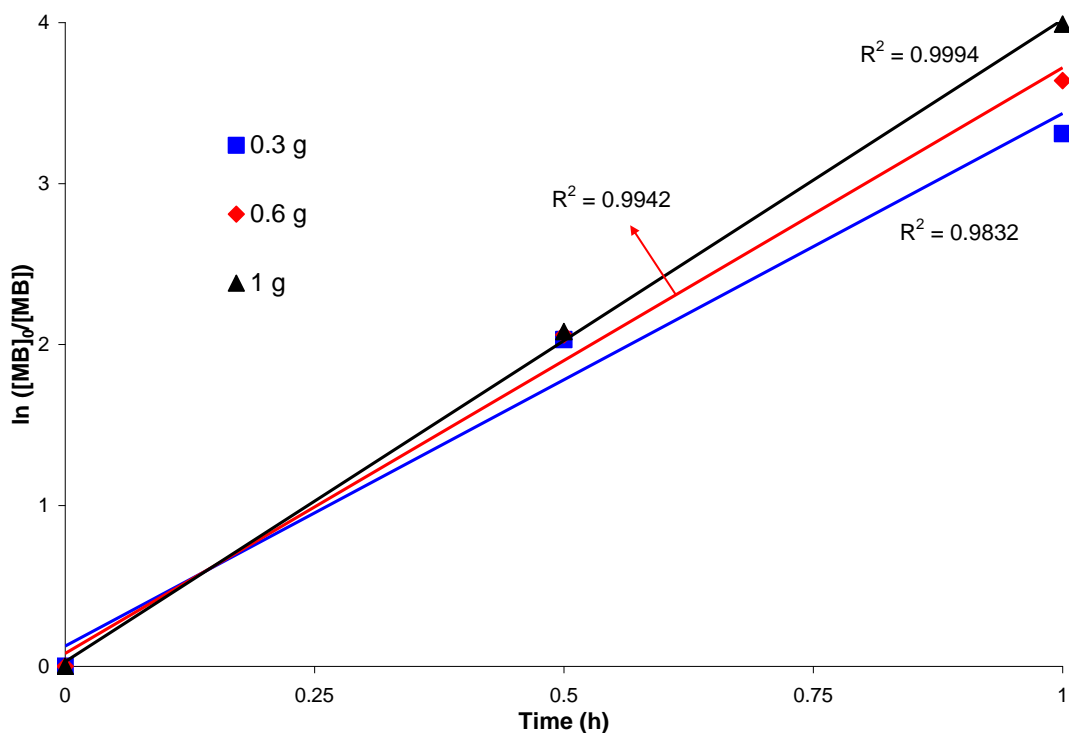


FIGURE 4. 21 Variation of $\ln([MB]_0/[MB])$ with UV exposure time for different amounts of 3HAP-TiO₂ in the solution

TABLE 4. 7 The reaction rate constant and correlation coefficient for different amounts of 3HAP-TiO₂ in the solution

	0.3 g TiO ₂	0.6 g TiO ₂	1 g TiO ₂
$K_{ap} (h^{-1})$	3.43	3.72	4.02
R^2	0.9832	0.9942	0.9994

As the amount of photocatalyst increases, the reaction rate also increases; in this case, from 3.43 for 0.3 g 3HAP-TiO₂, to 3.72 for 0.6 g 3HAP-TiO₂, and to 4.02 for 1 g 3HAP-TiO₂. The values of R^2 for each sample seem to be close to 1.0, which means that the decomposition of MB solution fits the Langmuir–Hinshelwood kinetic model.

CHAPTER V

CONCLUSIONS

1. Hydroxyapatite (HAP) could be successfully deposited on TiO_2 powders by a biomimetic process through immersing TiO_2 powders in simulated body fluid, SBF, containing calcium and phosphate ion concentrations 10 times greater than those of human blood plasma.
2. The immersion time has a profound effect on the amount of HAP deposition on TiO_2 powders. The 3 h immersion duration in 10-SBF offers the best results in terms of HAP deposition. Further immersion durations do not enhance HAP deposition.
3. The HAP deposition on the surface of TiO_2 powders delays the decomposition of poly(methyl methacrylate). Therefore, HAP deposited TiO_2 powders could be used to protect PMMA from photodecomposition.
4. The HAP deposition on the surface of TiO_2 powders improves the absorption ability of TiO_2 powders in dark, and the photocatalytic activity of TiO_2 powders in aqueous methylene blue (MB) solution.
5. UV light absorption and MB decomposition ability of HAP deposited TiO_2 powders increases with increasing HAP content on the surface.
6. The decomposition time of MB decreases as the amount of HAP deposited TiO_2 in the solution increases.

REFERENCES

- [1] A.J. Kay, "Design and Development of Two Large-scale Photocatalytic Reactors for Treatment of Toxic Organic Chemicals in Wastewater" in M. A. Abraham, R.P. Hesketh (eds.) *Reaction Engineering for Pollutions Prevention*, Amsterdam: Elsevier, (2000) pp: 155-171
- [2] H. Ibrahim, H. de Lasa, "Novel Photocatalytic Reactor for the Destruction of Airborne Pollutants" in M. A. Abraham, R.P. Hesketh (eds.) *Reaction Engineering for Pollutions Prevention*, Amsterdam: Elsevier, (2000) pp: 127-135
- [3] J. C. Crittenden, Y. Zhang, D. W. Hand, D. L. Perram, E. G. Marchand, "Solar Detoxification of Fuel-contaminated Groundwater Using Fixed-bed Photocatalysts" *Water Environment Research*, Volume 68, Issue 3, (1996) pp: 270-278
- [4] P. -Y. Maness, S. Smolinski, D. M. Blake, Z. Huang, E. J. Wolfrum, W. A. Jacoby, "Bactericidal Activity of Photocatalytic TiO₂ Reaction: Toward Understanding of its Killing Mechanism" *Applied and Environmental Microbiology*, Volume 65, Issue 9, (1999) pp: 4094-4098
- [5] E. Pelizzetti, C. Minero, H. Hidaka, N. Serpone, "Photocatalytic Processes for Surfactant Degradation" in D.F. Ollis, H. Al-Ekabi (eds.) *Photocatalytic Purification and Treatment of Water and Air*, Amsterdam: Elsevier, (1993) pp: 261- 273
- [6] C. Su, B.-Y. Hong, C.-M. Tseng "Sol-gel Preparation and Photocatalysis of Titanium Dioxide" *Catalysis Today*, Volume 96, Issue 3, (2004) pp: 119-126

- [7] Z. Yang, S. Si, X. Zeng, C. Zhang, H. Dai, "Mechanism and Kinetics of Apatite Formation on Nanocrystalline TiO₂ Coatings: A quartz crystal microbalance study" *Acta Biomaterialia*, Volume 4, Issue 3, (2008) pp: 560-568
- [8] D. D. Dionysiou, G. Balasubramanian, M. T. Suidan, I. Baudin, J.-M. Laine, "Thin Film Photocatalytic Reactor for the Destruction of Organic Contaminants in Industrial Wastewater and Drinking Water" in M. A. Abraham, R.P. Hesketh (eds.) *Reaction Engineering for Pollutions Prevention*, Amsterdam: Elsevier, (2000) pp: 137-153
- [9] A. Fujishima, T. N. Rao, D. A. Tryk, "Titanium Dioxide Photocatalysis" *Journal of Photochemistry and Photobiology C: Photochemistry Reviews*, Volume 1, Issue 1, (2000) pp: 1-21
- [10] D. W. Bahnemann, D. Bockelmann, R. Goslich, M. Hilgendorff, D. Weichgrebe, "Photocatalytic Detoxification: Novel Catalyst, Mechanism and Solar Applications" in D.F. Ollis, H. Al-Ekabi (eds.) *Photocatalytic Purification and Treatment of Water and Air*, Amsterdam: Elsevier, (1993) pp: 301- 319
- [11] T. Nonami, H. Hase, K. Funakoshi, "Apatite-Coated Titanium Dioxide Photocatalyst for Air Purification" *Catalysis Today*, Volume 96, Issue 3, (2004) pp: 113-118
- [12] W. Kangwansupamonkon, V. Lauruengtana, S. Surassmo, U. Ruktanonchai, "Antibacterial Effect of Apatite-Coated Titanium Dioxide for Textiles Applications" *Nanomedicine: Nanomedicine: Nanotechnology, Biology and Medicine*, Volume 5, Issue 2, (2009) pp: 240-249
- [13] T. Nonami, H. Taoda, N. T. Hue, E. Watanabe, K. Iseda, M. Tazawa, M. Fukaya, "Apatite Formation on TiO₂ Photocatalyst Film in a Pseudo Body Solution" *Materials Research Bulletin*, Volume 33, Issue 1, (1998) pp: 125-131.

- [14] T. Kokubo, H. -M. Kim, F. Miyaji, H. Takadama, T. Miyazaki, "Ceramic–Metal and Ceramic–Polymer Composites Prepared by a Biomimetic Process" *Composites Part A: Applied Science and Manufacturing*, Volume 30, Issue 4, (1999) pp: 405-409
- [15] S. Bharati, M. K. Sinha, D. Basu, "Hydroxyapatite Coating by Biomimetic Method on Titanium Alloy Using Concentrated SBF" *Bulletin of Material Science*, Volume 28, Issue 6, (2005) pp: 617–621
- [16] A. C. Tas, "Synthesis of Biomimetic Ca-Hydroxyapatite Powders at 373°C in Synthetic Body Fluids" *Biomaterials*, Volume 21, Issue 14, (2000) pp: 1429-1438
- [17] T. Kasuga, H. Kondo, M. Nogami, "Apatite Formation on TiO₂ in Simulated Body Fluid" *Journal of Crystal Growth*, Volume 235, Issues 1-4, (2002) pp: 235-240
- [18] A. Syoufian, K. Nakashima, "Degradation of Methylene Blue in Aqueous Dispersion of Hollow Titania Photocatalyst: Study of Reaction Enhancement by Various Electron Scavengers" *Journal of Colloid and Interface Science*, Volume 317, Issue 2, (2008) pp: 507-512
- [19] W.-C. Oh, A.-R. Jung, W.-B. Ko, "Characterization and Relative Photonic Efficiencies of a New Nanocarbon/TiO₂ Composite Photocatalyst Designed for Organic Dye Decomposition and Bactericidal Activity" *Materials Science and Engineering: C*, Volume 29, Issue 4, (2009) pp: 1338-1347
- [20] J. Grzechulska-Damszel, M. Tomaszewska, A.W. Morawski, "Integration of Photocatalysis with Membrane Processes for Purification of Water Contaminated with Organic Dyes" *Desalination*, Volume 241, Issues 1-3, (2009) pp: 118-126
- [21] D. F. Ollis, "Contaminant Degradation in Water, Heterogeneous Photocatalysis Degrades Halogenated Hydrocarbon" *Environmental Science & Technology*, Volume 19, Issue 1, (1985) pp: 480-484.

- [22] A. Fujishima, K. Honda, "Electrochemical Photolysis of Water at a Semiconductor Electrode" *Nature*, Volume 238, Issue 5358, (1972) pp: 37-38
- [23] H. de Lasa, B. Serrano, M. Salaiques, *Photocatalytic Reaction Engineering*, New York: Springer, (2005) p: 49
- [24] H. Gerischer, "Conditions for an Efficient Photocatalytic Activity of TiO₂ Particles" in D.F. Ollis, H. Al-Ekabi (eds.) *Photocatalytic Purification and Treatment of Water and Air*, Amsterdam: Elsevier, (1993) pp: 1-17
- [25] J.-M. Herrmann, C. Duchamp, M. Karkmaz, B. T. Hoai, H. Lachheb, E. Puzenat, C. Guillard "Environmental Green Chemistry as Defined by Photocatalysis" *Journal of Hazardous Materials*, Volume 146, Issue 3, (2007) pp: 624-629
- [26] K.-Ichi Okamoto, Y. Yamamoto, H. Tanaka, M. Tanaka, A. Itaya "Heterogeneous Photocatalytic Decomposition of Phenol over TiO₂ Powder" *Bulletin of the Chemical Society of Japan*, Volume 58, Issue 7, (1985) pp: 2015-2022
- [27] A. Heller, S. -E. Lindquist, "Photoassisted Oxidation of Oil and Organic Spills on Water" in D.F. Ollis, H. Al-Ekabi (eds.) *Photocatalytic Purification and Treatment of Water and Air*, Amsterdam: Elsevier, (1993) pp: 139-153
- [28] H. Yamashita, M. Harada, J. Misaka, M. Takeuchi, B. Neppolian, M. Anpo, "Photocatalytic Degradation of Organic Compounds Diluted in Water Using Visible Light-Responsive Metal Ion-Implanted TiO₂ Catalysts: Fe Ion-Implanted TiO₂" *Catalysis Today*, Volume 84, Issues 3-4, (2003) pp: 191-196
- [29] M.R. Prairie, B.M. Stange, L.R. Evans, "TiO₂ Catalysis for Destruction of Organics and the Reduction of Heavy Metals", in D.F. Ollis, H. Al-Ekabi (eds.) *Photocatalytic Purification and Treatment of Water and Air*, Amsterdam: Elsevier, (1993) pp: 353-363

[30] N. Serpone, E. Pelizzetti, H. Hidaka, "Identifying Primary Events and the Nature of Intermediates Formed during the Photocatalyzed Oxidation of Organics Mediated by Irradiated Semiconductors", in D.F. Ollis, H. Al-Ekabi (eds.) *Photocatalytic Purification and Treatment of Water and Air*, Amsterdam: Elsevier, (1993) pp: 225-250

[31] H. Hidaka, J. Zhao, K. Nohara, K. Kitamura, Y. Satoh, E. Pelizzetti, N. Serpone, "Photocatalyzed Mineralization of Non-Ionic, Cationic, and Anionic Surfactants at TiO₂/H₂O Interfaces", in D.F. Ollis, H. Al-Ekabi (eds.) *Photocatalytic Purification and Treatment of Water and Air*, Amsterdam: Elsevier, (1993) pp: 251-259

[32] Y. Mao, C. Schöneich, K.-D. Asmus, "Radical Mediated Degradation Mechanisms of Halogenated Organic Compounds As Studied by Photocatalysis at TiO₂ and by radiation chemistry", in D.F. Ollis, H. Al-Ekabi (eds.) *Photocatalytic Purification and Treatment of Water and Air*, Amsterdam: Elsevier, (1993) pp: 49-66

[33] R. P. S. Suri, J. Liu, D. W. Hand, J. C. Crittenden, D. L. Perram, M. E. Mullins "Heterogeneous Photocatalytic Oxidation of Hazardous Organic Contaminants in Water" *Water Environment Research*, Volume 65, Issue 5, (1993) pp: 665-673

[34] A. S. Grove, *Physics and Technology of Semiconductor Devices*, New York: Wiley & Sons Co., (1967) pp: 91-92

[35] T. İ. Ersöz, *Application of Semi-Conductor Films over Glass/Ceramic Surfaces and their Low Temperature Photocatalytic Activity*, MSc Thesis, METU Ankara, (2009) p: 13

[36] D. F. Ollis, C. -Y. Hsiao, L. Budiman, C. -L. Lee, "Heterogeneous Photoassisted Catalysis: Conversions of Perchloroethylene, Dichloroethane, Chloroacetic acids, and Chlorobenzenes" *Journal of Catalysis*, Volume 88, Issue 1, (1984) pp: 89-96

[37] R. W. Matthews, "Photocatalysis in Water Purification: Possibilities, Problems and Prospects" in D.F. Ollis, H. Al-Ekabi (eds.) *Photocatalytic Purification and Treatment of Water and Air*, Amsterdam: Elsevier, (1993) pp: 121-138

[38] S. I. Shah, W. Li, C.-P. Huang, O. Jung, C. Ni, "Study of Nd^{3+} , Pd^{2+} , Pt^{4+} , and Fe^{3+} Dopant Effect on Photoreactivity of TiO_2 Nanoparticles" *Proceedings of the National Academy of Sciences of the United States of America*, Volume 99, Issue 2, (2002) pp: 6482-6486

[39] J. Chen, D. F. Ollis, W. H. Rulkens, H. Bruning, "Photocatalyzed Oxidation of Alcohols and Organochlorides in the Presence of Native TiO_2 and Metallized TiO_2 Suspensions. Part (II): Photocatalytic Mechanisms" *Water Research*, Volume 33, Issue 3, (1999) pp: 669-676

[40] B. Guo, Z. Liu, L. Hong, H. Jiang, "Sol Gel Derived Photocatalytic Porous TiO_2 Thin Films" *Surface and Coatings Technology*, Volume 198, Issues 1-3, (2005) pp: 24-29

[41] K. Ozeki, Juliana M. Janurudin, H. Aoki, Y. Fukui "Photocatalytic Hydroxyapatite/Titanium Dioxide Multilayer Thin Film Deposited onto Glass Using an rf Magnetron Sputtering Technique" *Applied Surface Science*, Volume 253, Issue 7, (2007), pp: 3397-3401

[42] S. Bailliez, A. Nzihou. "The Kinetics of Surface Area Reduction During Isothermal Sintering of Hydroxyapatite Adsorbent" *Chemical Engineering Journal*, Volume 98, Issues 1-2, (2004) pp: 141-152

[43] S. Doonan, "Chromatography on Hydroxyapatite" in S. Doonan (ed.) *Protein Purification Protocols*, New Jersey: Humana Press, (1996) pp: 211-215

- [44] H. Anmin, L. Ming, C. Chengkang, M. Dali, "Preparation and Characterization of a Titanium-Substituted Hydroxyapatite Photocatalyst" *Journal of Molecular Catalysis A: Chemical*, Volume 267, Issues 1-2, (2007) pp: 79-85
- [45] D. McConnel, *Apatite: Its Crystal Chemistry, Mineralogy, Utilization, and Geologic and Biologic Occurrences*, New York: Springer-Verlag, (1973) p. 1
- [46] N. O. Engin, A. C. Tas, "Manufacture of Macroporous Calcium Hydroxyapatite Bioceramics" *Journal of the European Ceramic Society*, Volume 19, Issues 13-14, (1999) pp: 2569-2572
- [47] H. Nishikawa, "A High Active Type of Hydroxyapatite for Photocatalytic Decomposition of Dimethyl Sulfide under UV Irradiation" *Journal of Molecular Catalysis A: Chemical*, Volume 207, Issue 2, (2004) pp: 149-153
- [48] I. A. Osgerby, "ISCO Technology Overview: Do You Really Understand the Chemistry?" in E.J. Calabrese, P.T. Kosteki, J. Dragun (eds.) *Contaminated Soils, Sediments and Water*, New York: Springer, (2006) pp: 287-308
- [49] H. Nishikawa, "Radical Generation on Hydroxyapatite by UV Irradiation" *Materials Letters*, Volume 58, Issues 1-2, (2004) pp:14-16
- [50] F. Liang, L. Zhou, K. Wang, "Apatite Formation on Porous Titanium by Alkali and Heat-Treatment", *Surface and Coating Technology*, Volume 165, Issue 1, (2002) pp: 133-139)
- [51] T. Miyazaki, H. -M. Kim, T. Kokubo, C. Ohtsuki, H. Kato, T. Nakamura, "Mechanism of Bonelike Apatite Formation on Bioactive Tantalum Metal in a Simulated Body Fluid" *Biomaterials*, Volume 23, Issue 3, (2002) pp: 827-832

[52] D. Bayraktar, A. C. Tas, "Chemical Preparation of Carbonated Calcium Hydroxyapatite Powders at 37°C in Urea-Containing Synthetic Body Fluids" *Journal of the European Ceramic Society*, Volume 19, Issues 13-14, (1999) pp: 2573-2579

[53] T. Kokubo, "Surface Chemistry of Bioactive Glass-Ceramics" *Journal of Non-Crystalline Solids*, Volume 120, Issues 1-3, (1990) pp: 138-151

[54] X. Lu, Y. Leng, "Theoretical Analysis of Calcium Phosphate Precipitation in Simulated Body Fluid" *Biomaterials*, Volume 26, Issue 1, (2005) pp: 1097–1108

[55] A. Oyane, H. M. Kim, T. Furuya, T. Kokubo, T. Miyazaki, T. Nakamura, "Preparation and Assessment of Revised Simulated Body Fluids" *Journal of Biomedical Materials Research Part A*, Volume 65, Issue 1, (2003) pp: 188-195

[56] A. Chughtai, R. Marshall, G. H. Nancollas, "Complexes in Calcium Phosphate Solutions" *the Journal of Physical Chemistry*, Volume 72, Issue 1, (1968) pp: 208–211

[57] T. Kokubo, H. Takadama, "Simulated Body Fluid (SBF) As A Standard Tool to Test the Bioactivity of Implants", in M. Epple, E. Beuerlein (eds.) *Handbook of Biomineralization: Medical and Clinical Aspects*, Weinheim: Wiley-VCH, (2007) pp: 102.

[58] J. Wang, P. Layrolle, M. Stigter, K. de Groot, "Biomimetic and Electrolytic Calcium Phosphate Coatings on Titanium Alloy: Physicochemical Characteristics and Cell Attachment" *Biomaterials*, Volume 25, Issue 4, (2004) pp: 583-592

[59] Z. Yang, S. Si, X. Zeng, C. Zhang, H. Dai, "Mechanism and Kinetics of Apatite Formation on Nanocrystalline TiO₂ Coatings: A Quartz Crystal Microbalance Study" *Acta Biomaterialia*, Volume 4, Issue 3, (2008) pp: 560-568

- [60] A. Mills, J. Wang, "Photobleaching of Methylene Blue Sensitised by TiO₂: an Ambiguous System?" *Journal of Photochemistry and Photobiology A: Chemistry*, Volume 127, Issues 1-3, (1999) pp: 123-134
- [61] J. E. Valladares, J. R. Bolton, "A Method for the Determination of Quantum Yields in Heterogeneous Systems: the TiO₂ Photocatalyzed Bleaching of Methylene Blue" in D.F. Ollis, H. Al-Ekabi (eds.) *Photocatalytic Purification and Treatment of Water and Air*, Amsterdam: Elsevier, (1993) pp: 111-120
- [62] K. V. Kumar, K. Porkodi, F. Rocha, "Langmuir–Hinshelwood Kinetics – A Theoretical Study", *Catalysis Communications*, Volume 9, Issue 5, (2008) pp: 82-84
- [63] K. -H. Wang, Y. -H. Hsieh, M. -Y. Chou, C. -Y. Chang, "Photocatalytic Degradation of 2-chloro and 2-nitrophenol by Titanium Dioxide Suspensions in Aqueous Solution" *Applied Catalysis B: Environmental*, Volume 21, Issue 1, (1999) pp: 1-8
- [64] R. A. Glennon, R. Young, M. Dukat, Y. Cheng, "Initial Characterization of PMMA as a Discriminative Stimulus" *Pharmacology Biochemistry and Behavior*, Volume 57, Issues 1-2, (1997) pp: 151-158
- [65] L. Rizzo, J. Koch, V. Belgiorno, M.A. Anderson "Removal of Methylene Blue in a Photocatalytic Reactor Using Polymethylmethacrylate Supported TiO₂ Nanofilm" *Desalination*, Volume 211, Issues 1-3, (2007) pp: 1-9
- [66] K. Iketani, R. -D. Sun, M. Toki, K. Hirota, O. Yamaguch, "Sol–gel-Derived TiO₂/poly(dimethylsiloxane) Hybrid Films and their Photocatalytic Activities" *Journal of Physics and Chemistry of Solids*, Volume 64, Issue 3, (2003) pp: 507-513

- [67] D. Hufschmidt, D. Bahnemann, J. J. Testa, C. A. Emilio, M. I. Litter, "Enhancement of the Photocatalytic Activity of Various TiO₂ Materials by Platinisation" *Journal of Photochemistry and Photobiology A: Chemistry*, Volume 148, Issues 1-3, (2002) pp: 223-231
- [68] T. Tachikawa, T. Majima, "Single-Molecule Fluorescence Imaging Techniques for the Detection of Reactive Oxygen Species" in A. Mendez-Vilas and J. Diaz (eds.) *Modern Research and Educational Topics in Microscopy*, Spain: Formatex, (2007)pp: 651-659
- [69], NANO Technologies, "Photocatalyst TiO₂ Raw Material" *NANO-SCR Catalyst Total Service Solution*, <http://www.nanoin.com/> (accessed April 7, 2010)
- [70] A. C. Tas, S. B. Bhaduri, "Rapid Coating of Ti6Al4V at Room Temperature with a Calcium Phosphate Solution Similar to 10×SBF" *Journal of Materials Research*, Volume 19, Issue 1, (2004) pp: 2742–2749.
- [71] M. Keshmiri, T. Troczynski, "Apatite Formation on TiO₂ Anatase Microspheres" *Journal of Non-Crystalline Solids*, Volume 324, Issue 1, (2003) pp: 289-294
- [72] J. Shi, C. Ding, Y. Wu, "Biomimetic Apatite Layers on Plasma-Sprayed Titanium Coatings after Surface Modification" *Surface and Coatings Technology*, Volume 137, Issue 1, (2001) pp: 97-103
- [73] Y. T. Xie, X. Y. Liu, P. K. Chu, C. X. Ding, "Nucleation and Growth of Calcium-Phosphate on Ca-Implanted Titanium Surface" *Surface Science*, Volume 600, (2006) pp: 651-656
- [74] Y. W. Gu, B. Y. Tay, C. S. Lim, M. S. Yong, "Biomimetic Deposition of Apatite Coating on Surface-Modified NiTi Alloy" *Biomaterials*, Volume 26, (2005) pp: 6916-6923

[75] R. Vinu, G. Madras, "Photocatalytic Degradation of Methyl Methacrylate Copolymers" *Polymer Degradation and Stability*, Volume 93, Issue 8, (2008) pp: 1440-1449

[76] S. -M. Yun, K. Palanivelu, Y. -H. Kim, P. -H. Kang, Y. -S. Lee, "Preparation and Characterization of Carbon Covered TiO₂ Using Sucrose for Solar Photodegradation" *Journal of Industrial and Engineering Chemistry*, Volume 14, Issue 5, (2008) pp: 667-671

[77] J. Park, "Photocatalytic Activity of Hydroxyapatite-Precipitated Potassium Titanate Whiskers" *Journal of Alloys and Compounds*, Volume 492, Issues 1-2, (2010) pp: 57-60

[78] N. Shimizu, C. Ogino, M. F. Dadjour, T. Murata, "Sonocatalytic Degradation of Methylene Blue with TiO₂ Pellets in Water" *Ultrasonics Sonochemistry*, Volume 14, Issue 2, (2007) pp: 184-190